Universität Karlsruhe (TH)
Institut für Baustatik

A mixed shell formulation accounting for thickness strains and finite strain 3d-material models

S. Klinkel, F. Gruttmann, W. Wagner

Mitteilung 4(2006)

Universität Karlsruhe (TH)
Institut für Baustatik

A mixed shell formulation accounting for thickness strains and finite strain 3d-material models

S. Klinkel, F. Gruttmann, W. Wagner

Mitteilung 4(2006)

Prof. Dr.–Ing. W. Wagner
Institut für Baustatik
Universität Karlsruhe
Postfach 6980
76128 Karlsruhe

Telefon: (0721) 608–2280
Telefax: (0721) 608–6015
E–mail: bs@.uni-karlsruhe.de
Internet: http://www.bs.uni-karlsruhe.de

A mixed shell formulation accounting for thickness strains and finite strain 3d-material models

Sven Klinkel*, Friedrich Gruttmann+, Werner Wagner*

* Institut für Baustatik, Universität Karlsruhe (TH), Kaiserstr. 12, 76131 Karlsruhe, Germany

+ Institut für Werkstoffe und Mechanik im Bauwesen, Technische Universität Darmstadt, Petersenstr. 12, 64287 Darmstadt, Germany

Contents

Summary A nonlinear quadrilateral shell element for the analysis of thin structures is presented. The Reissner–Mindlin theory with inextensible director vector is used to develop a three–field variational formulation with independent displacements, stress resultants and shell strains. The interpolation of the independent shell strains consists of two parts. The first part corresponds to the interpolation of the stress resultants. Within the second part independent thickness strains are considered. This allows incorporation of arbitrary nonlinear three-dimensional constitutive equations without further modifications. The developed mixed hybrid shell element possesses the correct rank and fulfills the in-plane and bending patch test. The essential feature of the new element is the robustness in the equilibrium iterations. It allows very large load steps in comparison to other element formulations. We present results for finite strain elasticity, inelasticty, bifurcation and post–buckling problems.

Key words: Reissner–Mindlin shell theory, three–field variational formulation, quadrilateral shell element, thickness strains, three–dimensional constitutive behavior

1 Introduction

In the past several papers on shell formulations accounting for finite strains have been published. As an example we mention [1], where the Mooney-Rivlin material involving large membrane strains has been implemented in a finite shell element. The zero normal stress condition in thickness direction is enforced with an update of the thickness change at the end of each equilibrium iteration. In [2] an algorithm to satisfy the stress condition was proposed, which requires the storage of some history variables on the element level. An approach with a quadratically convergent iteration at each integration point has been developed in [3] and generalized in [4].
A further possibility to introduce 3d–material laws is to use a higher–order shell model with extensible director kinematic. In the literature there is general agreement that formulations accounting for the through–the–thickness strain should represent the normal strain in thickness direction E_{33} at least linear through the shell thickness, e.g. [5, 6]. This can be achieved assuming a quadratic distribution of the displacements through the thickness, e.g. [7, 8]. This approach leads to a finite element formulation with seven parameters at the nodes (three displacements of the mid-surface, two rotational parameters and two through–the–thickness stretching parameters). Another way is to enhance the thickness strains e.g. [9, 10, 11] applying the enhanced assumed strain method (EAS–method) [12]. The associated finite element possesses six displacement–like parameters at the nodes and a strain-like through–the–thickness variable, which is condensed out at the element level. Comparisons of both approaches are given in [6]. A 5–parameter shell element is developed by Huettel and Matzenmiller [13] using the EAS-approach and a polynomial expansion of the thickness strains with constant and linear parts. The associated parameters are eliminated at element level.

Based on this preliminary discussion the new aspects and essential features of the paper are summarized as follows:

(i) The present nonlinear finite rotation shell theory is based on the Reissner–Mindlin kinematic with inextensible director vector and constant transverse shear strains through the thickness. That is, the kinematic assumption leads to vanishing thickness strains when exploiting the Green–Lagrangean strain tensor. We derive the variational formulation of the boundary value problem using the static and kinematic field equations and the constitutive equations. Within a three–field formulation the displacement field, the stress resultants and the shell strains are introduced as independent tensorial quantities. The finite element formulation for quadrilaterals using the isoparametric concept is explicitly described.

(ii) Based on a previous publication [14], where appropriate interpolation functions for the stress resultants and shell strains are given, we present several new aspects. The strain interpolation is enhanced as follows. The approximation consists of two parts. The first part is identical to the shape functions for the stress resultants and the functions of the second part are constructed orthogonal to the stress interpolation functions. Within this concept independent thickness strains using one, two or eight parameters can easily be incorporated. The second part of the strain interpolation for the membrane and bending part leads to an improvement of the element behavior especially when coupling of the membrane and bending stiffness occurs. This is e.g. the case for arbitrary nonlinear constitutive behavior or for laminated shells with certain layer sequences. An effective procedure to eliminate the stress and strain parameters avoiding expensive matrix inversions is presented. Static condensation of a certain number of parameters is achieved applying a Gaussian elimination procedure.

(iii) Using above mixed hybrid element description the developed finite shell element allows consideration of arbitrary nonlinear three–dimensional constitutive equations without further modifications. The resultants of the thickness normal stresses are set to zero within the Euler–Lagrange equation and thus approach zero within the finite element solution and mesh refinement. This can be interpreted as an average fulfillment of the zero normal stress condition for each element.

(iv) Shell intersections are possible using 6 degrees of freedom (three displacements and three global rotations) at nodes on intersections and 5 degrees of freedoms (three displacements and two local rotations) at other nodes. This is an essential advantage in contrast to above discussed shell formulations with extensible director vectors and thickness strains at the nodes, which leads to difficulties along with shell intersections. The problem follows from continuity of extensible director vector or thickness strain at the intersection nodes, which may lead to wrong results.

(v) The developed element undergoes several test problems. The element stiffness matrix possesses the correct rank and fulfills the membrane and bending patch test. We investigate the nonlinear behavior of thin structures including stability. Furthermore Ogden´s material law and finite strain inelasticity are considered as nonlinear constitutive equations. The computed examples show the robustness especially in the equilibrium iterations. The element allows very large load steps in comparison to other element formulations.

2 Variational formulation of the shell equations

Let $\mathcal{B}$ be the three–dimensional Euclidean space occupied by the shell in the reference configuration. With ξ^i and $\mathbf{e}_i$ we denote a convected coordinate system of the body and the global cartesian basis system, respectively. The thickness coordinate $\xi^3 = 0$ with $h_- \leq \xi^3 \leq h_+$ defines the arbitrary reference surface Ω with boundary Γ. The initial shell thickness is given by h. The position vectors of the initial reference surface and current surface are denoted by $\mathbf{X}(\xi^1, \xi^2)$ and $\mathbf{x}(\xi^1, \xi^2)$, respectively. Furthermore, a director vector $\mathbf{D}(\xi^1, \xi^2)$ with $|\mathbf{D}(\xi^1, \xi^2)| = 1$ is introduced as a vector perpendicular to Ω. The unit director $\mathbf{d}$ of the current configuration is obtained by an orthogonal transformation. In the following the summation convention is used for repeated indices, where Latin indices range from 1 to 3 and Greek indices range from 1 to 2. Commas denote partial differentiation with respect to the coordinates ξ^α. With $\mathbf{d} \cdot \mathbf{x}_{,\alpha} \neq 0$ we account for transverse shear strains within a Reissner-Mindlin theory. The shell is loaded statically by surface loads $\bar{\mathbf{p}}$ on Ω and by boundary forces $\bar{\mathbf{t}}$ on Γ_σ. Furthermore, displacements $\bar{\mathbf{u}}$ and rotations $\bar{\boldsymbol{\omega}}$ are prescribed on Γ_u, where $\Gamma = \Gamma_\sigma \bigcup \Gamma_u$. Using the mentioned kinematic assumption the membrane strains $\varepsilon_{\alpha\beta}$, curvatures $\kappa_{\alpha\beta}$ and shear strains γ_α are given, see e.g. [15]

$$\begin{aligned} \varepsilon_{\alpha\beta} &= \frac{1}{2}(\mathbf{x}_{,\alpha} \cdot \mathbf{x}_{,\beta} - \mathbf{X}_{,\alpha} \cdot \mathbf{X}_{,\beta}) \\ \kappa_{\alpha\beta} &= \frac{1}{2}(\mathbf{x}_{,\alpha} \cdot \mathbf{d}_{,\beta} + \mathbf{x}_{,\beta} \cdot \mathbf{d}_{,\alpha} - \mathbf{X}_{,\alpha} \cdot \mathbf{D}_{,\beta} - \mathbf{X}_{,\beta} \cdot \mathbf{D}_{,\alpha}) \\ \gamma_\alpha &= \mathbf{x}_{,\alpha} \cdot \mathbf{d} - \mathbf{X}_{,\alpha} \cdot \mathbf{D} \,. \end{aligned} \tag{1}$$

The shell strains depend on $\mathbf{v}^T = [\mathbf{u}^T, \boldsymbol{\omega}^T]$ with displacements $\mathbf{u} = \mathbf{x} - \mathbf{X}$ and rotational parameters $\boldsymbol{\omega}$ of the reference surface. The components are organized in a vector

$$\boldsymbol{\varepsilon}_g(\mathbf{v}) = [\varepsilon_{11}, \varepsilon_{22}, 2\varepsilon_{12}, \kappa_{11}, \kappa_{22}, 2\kappa_{12}, \gamma_1, \gamma_2]^T \tag{2}$$

where the subscript g indicates geometric strains as function of the displacement field. The associated variation is given by $\delta\boldsymbol{\varepsilon}_g = [\delta\varepsilon_{11}, \delta\varepsilon_{22}, 2\delta\varepsilon_{12}, \delta\kappa_{11}, \delta\kappa_{22}, 2\delta\kappa_{12}, \delta\gamma_1, \delta\gamma_2]^T$

$$\begin{aligned} \delta\varepsilon_{\alpha\beta} &= \frac{1}{2}(\delta\mathbf{x}_{,\alpha} \cdot \mathbf{x}_{,\beta} + \delta\mathbf{x}_{,\beta} \cdot \mathbf{x}_{,\alpha}) \\ \delta\kappa_{\alpha\beta} &= \frac{1}{2}(\delta\mathbf{x}_{,\alpha} \cdot \mathbf{d}_{,\beta} + \delta\mathbf{x}_{,\beta} \cdot \mathbf{d}_{,\alpha} + \delta\mathbf{d}_{,\alpha} \cdot \mathbf{x}_{,\beta} + \delta\mathbf{d}_{,\beta} \cdot \mathbf{x}_{,\alpha}) \\ \delta\gamma_\alpha &= \delta\mathbf{x}_{,\alpha} \cdot \mathbf{d} + \delta\mathbf{d} \cdot \mathbf{x}_{,\alpha} \,. \end{aligned} \tag{3}$$

We postulate the existence of a strain energy density $\hat{W}(\mathbf{C})$ as function of the right Cauchy-Green tensor $\mathbf{C} = \mathbf{F}^T\mathbf{F}$ with the deformation gradient $\mathbf{F}$. The components of the Green–Lagrangean strain tensor $\mathbf{E} = \frac{1}{2}(\mathbf{C} - \mathbf{1})$ are written in vector form $\mathbf{E} = [E_{11}, E_{22}, E_{33}, 2E_{12}, 2E_{13}, 2E_{23}]^T$ and the relation to the independent shell strains is defined by

$$\mathbf{E} = \mathbf{A}\,\boldsymbol{\varepsilon} \qquad \mathbf{A} = [\mathbf{A}_1, \mathbf{A}_2]$$

$$\mathbf{A}_1 = \begin{bmatrix} 1 & 0 & 0 & \xi^3 & 0 & 0 & 0 & 0 \\ 0 & 1 & 0 & 0 & \xi^3 & 0 & 0 & 0 \\ 0 & 0 & 0 & 0 & 0 & 0 & 0 & 0 \\ 0 & 0 & 1 & 0 & 0 & \xi^3 & 0 & 0 \\ 0 & 0 & 0 & 0 & 0 & 0 & 1 & 0 \\ 0 & 0 & 0 & 0 & 0 & 0 & 0 & 1 \end{bmatrix} \quad \mathbf{A}_2 = \begin{bmatrix} 0 & 0 \\ 0 & 0 \\ 1 & \xi^3 \\ 0 & 0 \\ 0 & 0 \\ 0 & 0 \end{bmatrix} \quad \boldsymbol{\varepsilon} = \begin{bmatrix} \boldsymbol{\varepsilon}_p \\ \boldsymbol{\varepsilon}_z \end{bmatrix} \quad \boldsymbol{\varepsilon}_z = \begin{bmatrix} \varepsilon^0_{33} \\ \varepsilon^1_{33} \end{bmatrix} \tag{4}$$

Here $\boldsymbol{\varepsilon}_p$ contains the shells strains in the arrangement according to Eq. (2), where the subscript p indicates physical strains which are related to the constitutive equations. Furthermore, ε^0_{33}, ε^1_{33} denote the constant and linear part of the independent thickness strains, respectively. The associated variation reads $\delta\mathbf{E} = \mathbf{A}\,\delta\boldsymbol{\varepsilon}$.
We continue with the internal virtual work of the shell considering $dV = \bar{\mu}\; d\xi^3\; dA$

$$\delta W_i = \int\limits_{(\Omega)} \int\limits_{(h)} \delta\hat{W}(\mathbf{C})\,\bar{\mu}\; d\xi^3\; dA = \int\limits_{(\Omega)} \delta\boldsymbol{\varepsilon}^T\,\partial_{\boldsymbol{\varepsilon}} W\; dA \tag{5}$$

with the area element $dA = j\, d\xi^1\, d\xi^2$, where $j = |\mathbf{X}_{,1} \times \mathbf{X}_{,2}|$ and the determinant of the shifter tensor $\bar{\mu}$. Considering $\delta\hat{W}(\mathbf{C}) = 2\delta\mathbf{E} : \partial_{\mathbf{C}}\hat{W}(\mathbf{C}) = (\mathbf{A}\delta\boldsymbol{\varepsilon}) : 2\partial_{\mathbf{C}}\hat{W}(\mathbf{C})$ in (5) yields the vector of the stress resultants

$$\partial_{\boldsymbol{\varepsilon}} W = \begin{bmatrix} \partial_{\boldsymbol{\varepsilon}_p} W \\ \partial_{\boldsymbol{\varepsilon}_z} W \end{bmatrix} := \int\limits_{h_-}^{h_+} \begin{bmatrix} \mathbf{A}_1^T \\ \mathbf{A}_2^T \end{bmatrix} \mathbf{S}\,\bar{\mu}\; d\xi^3 \tag{6}$$

with the Second Piola–Kirchhoff stresses $\mathbf{S} = 2\,\partial_{\mathbf{C}}\hat{W}(\mathbf{C})$.
In the following we summarize the static and geometric field equations and the constitutive equations as follows, [15]

$$\left.\begin{aligned} \tfrac{1}{j}\,(j\,\mathbf{n}^\alpha)_{,\alpha} + \bar{\mathbf{p}} &= \mathbf{0} & \qquad \boldsymbol{\varepsilon}_g - \boldsymbol{\varepsilon}_p &= \mathbf{0} \\ \tfrac{1}{j}\,(j\,\mathbf{m}^\alpha)_{,\alpha} + \mathbf{x}_{,\alpha} \times \mathbf{n}^\alpha &= \mathbf{0} & \qquad \partial_{\boldsymbol{\varepsilon}_p} W - \boldsymbol{\sigma} &= \mathbf{0} \\ & & \qquad \partial_{\boldsymbol{\varepsilon}_z} W &= \mathbf{0} \end{aligned}\right\} \quad \text{in } \Omega\,. \tag{7}$$

Here we denote by $\boldsymbol{\sigma}$ the vector of independent stress resultants

$$\boldsymbol{\sigma} = [n^{11}, n^{22}, n^{12}, m^{11}, m^{22}, m^{12}, q^1, q^2]^T \tag{8}$$

with membrane forces $n^{\alpha\beta} = n^{\beta\alpha}$, bending moments $m^{\alpha\beta} = m^{\beta\alpha}$ and shear forces q^α. The quantities $n^{\alpha\beta}$ and q^α are effective stress resultants which are related to the integrals of the First Piola–Kirchhoff stress tensor by well-known transformations. Furthermore it holds $\mathbf{n}^\alpha := n^{\alpha\beta}\,\mathbf{x}_{,\beta} + q^\alpha\,\mathbf{d} + m^{\alpha\beta}\,\mathbf{d}_{,\beta}$, $\mathbf{m}^\alpha := \mathbf{d} \times m^{\alpha\beta}\,\mathbf{x}_{,\beta}$.
The static and geometric boundary conditions read

$$\begin{aligned} j\,(\mathbf{n}^\alpha\,\nu_\alpha) - \bar{\mathbf{t}} &= \mathbf{0} \quad , \quad j\,(\mathbf{m}^\alpha\,\nu_\alpha) = \mathbf{0} \qquad \text{on} \quad \Gamma_\sigma \\ \mathbf{v} - \bar{\mathbf{v}} &= \mathbf{0} \qquad\qquad\qquad\qquad\quad \text{on} \quad \Gamma_u \end{aligned} \tag{9}$$

where ν_α denote the components of the normal vector on the shell boundary and $\bar{\mathbf{v}}^T = [\bar{\mathbf{u}}^T, \bar{\boldsymbol{\omega}}^T]$. We introduce $\boldsymbol{\theta} := [\mathbf{v}, \boldsymbol{\sigma}, \boldsymbol{\varepsilon}]^T$, the associated virtual quantities $\delta\boldsymbol{\theta} := [\delta\mathbf{v}, \delta\boldsymbol{\sigma}, \delta\boldsymbol{\varepsilon}]^T$ with $\delta\mathbf{v} = [\delta\mathbf{u}, \delta\boldsymbol{\omega}]^T$. Hence, the associated weak form of the boundary value problem is given in a standard way

$$\begin{aligned} g(\boldsymbol{\theta}, \delta\boldsymbol{\theta}) \;=\; & \int\limits_{(\Omega)} [\delta\boldsymbol{\varepsilon}_p^T(\partial_{\boldsymbol{\varepsilon}_p} W - \boldsymbol{\sigma}) + \delta\boldsymbol{\varepsilon}_z^T \partial_{\boldsymbol{\varepsilon}_z} W + \delta\boldsymbol{\sigma}^T(\boldsymbol{\varepsilon}_g - \boldsymbol{\varepsilon}_p)]\; dA \\ & - \int\limits_{(\Omega)} [(\frac{1}{j}\,(j\,\mathbf{n}^\alpha)_{,\alpha} + \bar{\mathbf{p}}) \cdot \delta\mathbf{u} + (\frac{1}{j}\,(j\,\mathbf{m}^\alpha)_{,\alpha} + \mathbf{x}_{,\alpha} \times \mathbf{n}^\alpha) \cdot \delta\boldsymbol{\omega}]\; dA = 0 \end{aligned} \tag{10}$$

Integration by parts of the second integral in (10) and incorporation of the static boundary conditions yields

$$
\begin{aligned}
g(\boldsymbol{\theta}, \delta\boldsymbol{\theta}) \;=\; & \int_{(\Omega)} [\delta\boldsymbol{\varepsilon}^T(\partial_{\boldsymbol{\varepsilon}} W - \tilde{\boldsymbol{\sigma}}) + \delta\boldsymbol{\sigma}^T(\boldsymbol{\varepsilon}_g - \boldsymbol{\varepsilon}_p) + \delta\boldsymbol{\varepsilon}_g^T\boldsymbol{\sigma}]\, dA \\
& - \int_{(\Omega)} \delta\mathbf{u}^T \bar{\mathbf{p}}\, dA - \int_{(\Gamma_\sigma)} \delta\mathbf{u}^T\, \bar{\mathbf{t}}\, ds = 0
\end{aligned}
\tag{11}
$$

with $\tilde{\boldsymbol{\sigma}} = [\boldsymbol{\sigma}, \mathbf{0}_2]^T$, which implies that the integral of S^{33} through the thickness is zero. The geometric boundary conditions have to be fulfilled as constraints.

3 Finite Element Equations

3.1 Interpolation of the initial and current reference surface

In this section the finite element equations for quadrilaterals are specified applying the isoparametric concept. The local numbering of the corner nodes and midside node can be seen in Fig. 1.

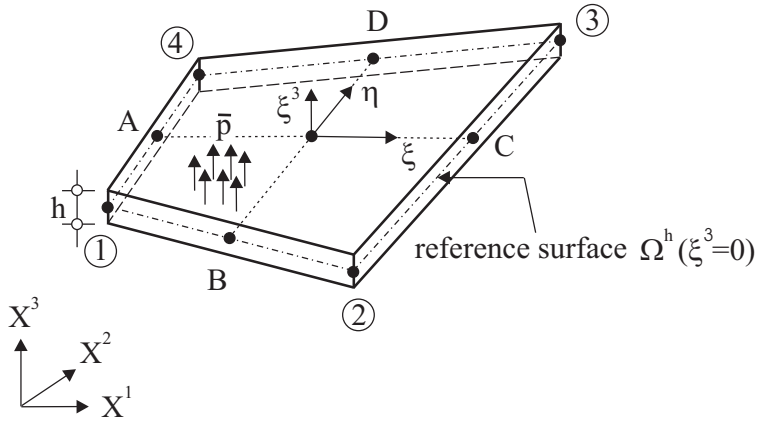

Figure 1: Quadrilateral shell element

A map of the coordinates $\{\xi, \eta\} \in [-1, 1]$ from the unit square to the reference surface in the initial and current configuration is applied. Thus the position vector and the director vector of the reference surface are interpolated with bi–linear functions

$$
\mathbf{X}^h = \sum_{I=1}^{4} N_I\, \mathbf{X}_I \qquad \mathbf{D}^h = \sum_{I=1}^{4} N_I\, \mathbf{D}_I \qquad N_I = \frac{1}{4}(1 + \xi_I\xi)(1 + \eta_I\eta) \tag{12}
$$

with $\xi_I \in \{-1, \;\; 1, \;\; 1, -1\}$ and $\eta_I \in \{-1, -1, \;\; 1, \;\; 1\}$. The superscript h denotes the characteristic size of the element discretization and indicates the finite element approximation. The nodal position vectors $\mathbf{X}_I$ and the local cartesian basis systems $[\mathbf{A}_{1I}, \mathbf{A}_{2I}, \mathbf{A}_{3I}]$ are generated within the mesh input. Here, $\mathbf{D}_I = \mathbf{A}_{3I}$ is perpendicular to Ω and $\mathbf{A}_{1I}$, $\mathbf{A}_{2I}$ are constructed in such a way that the boundary conditions can be accommodated. With $(12)_2$ the orthogonality is only given at the nodes.

For each element a local cartesian basis $\mathbf{t}_i$ is evaluated

$$\begin{aligned} \bar{\mathbf{d}}_1 &= \mathbf{X}_3 - \mathbf{X}_1 & \widehat{\mathbf{d}}_{\mathbf{1}} &= \bar{\mathbf{d}}_1/|\bar{\mathbf{d}}_1| \\ \bar{\mathbf{d}}_2 &= \mathbf{X}_2 - \mathbf{X}_4 & \widehat{\mathbf{d}}_{\mathbf{2}} &= \bar{\mathbf{d}}_2/|\bar{\mathbf{d}}_2| \\ \mathbf{t}_1 &= (\widehat{\mathbf{d}}_{\mathbf{1}} + \widehat{\mathbf{d}}_{\mathbf{2}})/|\widehat{\mathbf{d}}_{\mathbf{1}} + \widehat{\mathbf{d}}_{\mathbf{2}}| \\ \mathbf{t}_2 &= (\widehat{\mathbf{d}}_{\mathbf{1}} - \widehat{\mathbf{d}}_{\mathbf{2}})/|\widehat{\mathbf{d}}_{\mathbf{1}} - \widehat{\mathbf{d}}_{\mathbf{2}}| \\ \mathbf{t}_3 &= \mathbf{t}_1 \times \mathbf{t}_2 \,. \end{aligned} \tag{13}$$

Hence the Jacobian matrix $\mathbf{J}$ is defined

$$\mathbf{J} = \begin{bmatrix} \mathbf{X}^h_{;\xi} \cdot \mathbf{t}_1 & \mathbf{X}^h_{;\xi} \cdot \mathbf{t}_2 \\ \mathbf{X}^h_{;\eta} \cdot \mathbf{t}_1 & \mathbf{X}^h_{;\eta} \cdot \mathbf{t}_2 \end{bmatrix} \tag{14}$$

with

$$\begin{aligned} \mathbf{X}^h_{;\xi} &= \mathbf{G}^0_\xi + \eta\, \mathbf{G}^1 & \mathbf{G}^0_\xi &= \frac{1}{4}\sum_{I=1}^{4} \xi_I\, \mathbf{X}_I \\ \mathbf{X}^h_{;\eta} &= \mathbf{G}^0_\eta + \xi\, \mathbf{G}^1 & \mathbf{G}^0_\eta &= \frac{1}{4}\sum_{I=1}^{4} \eta_I\, \mathbf{X}_I \\ & & \mathbf{G}^1 &= \frac{1}{4}\sum_{I=1}^{4} \xi_I\, \eta_I\, \mathbf{X}_I \,. \end{aligned} \tag{15}$$

One can prove that $\mathbf{t}_3 \cdot \mathbf{G}^0_\xi = 0$ and $\mathbf{t}_3 \cdot \mathbf{G}^0_\eta = 0$ holds which shows that $\mathbf{t}_3$ is a normal vector at the element center. Thus $\mathbf{t}_1$ and $\mathbf{t}_2$ span a tangent plane at the center of the element. Now we are able to express the local cartesian derivatives of the shape functions using the inverse Jacobian matrix $\mathbf{J}$. The tangent vectors $\mathbf{X}_{,\alpha}$ and the derivatives of the director vector $\mathbf{D}_{,\alpha}$ are computed considering (12) as follows

$$\mathbf{X}^h_{;\alpha} = \sum_{I=1}^{4} N_{I,\alpha}\, \mathbf{X}_I \qquad \mathbf{D}^h_{;\alpha} = \sum_{I=1}^{4} N_{I,\alpha}\, \mathbf{D}_I \qquad \begin{bmatrix} N_{I,1} \\ N_{I,2} \end{bmatrix} = \mathbf{J}^{-1} \begin{bmatrix} N_{I,\xi} \\ N_{I,\eta} \end{bmatrix} . \tag{16}$$

For arbitrary warped elements one obtains $\mathbf{X}^h_{;\alpha} = \mathbf{t}_\alpha$ at the element center, which can be shown using above orthogonality conditions. This is important in the context of the present mixed interpolation. Furthermore a local cartesian system is advantageous to verify complicated nonlinear constitutive equations. At other points of the element the vectors $\mathbf{X}^h_{;\alpha}$ are only approximately orthogonal.

The current shell middle surface is approximated in the same way

$$\begin{aligned} \mathbf{x}^h &= \sum_{I=1}^{4} N_I\, \mathbf{x}_I & \mathbf{d}^h &= \sum_{I=1}^{4} N_I\, \mathbf{d}_I \\ \mathbf{x}^h_{;\alpha} &= \sum_{I=1}^{4} N_{I,\alpha}\, \mathbf{x}_I & \mathbf{d}^h_{;\alpha} &= \sum_{I=1}^{4} N_{I,\alpha}\, \mathbf{d}_I \,, \end{aligned} \tag{17}$$

where $\mathbf{x}_I = \mathbf{X}_I + \mathbf{u}_I$ describes the current nodal position vector and $\mathbf{d}_I = \mathbf{a}_{3I}$ is obtained by an orthogonal transformation $\mathbf{a}_{kI} = \mathbf{R}_I\,\mathbf{A}_{kI}, \quad k = 1,2,3$. The rotation tensor $\mathbf{R}_I$ is a function of the parameters ω_{kI} organized in the vector $\boldsymbol{\omega}_I = [\omega_{1I}, \omega_{2I}, \omega_{3I}]^T$ and is evaluated via Rodrigues' formula

$$\mathbf{R}_I = \mathbf{1} + \frac{\sin\omega_I}{\omega_I}\boldsymbol{\Omega}_I + \frac{1-\cos\omega_I}{\omega_I^2}\boldsymbol{\Omega}_I^2 \qquad \boldsymbol{\Omega}_I = \operatorname{skew}\boldsymbol{\omega}_I = \begin{bmatrix} 0 & -\omega_{3I} & \omega_{2I} \\ \omega_{3I} & 0 & -\omega_{1I} \\ -\omega_{2I} & \omega_{1I} & 0 \end{bmatrix}. \tag{18}$$

Representation (18) is singularity free for $\omega_I = |\boldsymbol{\omega}_I| < 2\pi$ which can always be fulfilled if after a certain number of load steps a multiplicative update of the total rotation tensor is applied.

The element has to fulfil membrane and bending patch test. The bending patch test – when using below defined mixed interpolation for the stress resultants and shell strains – can be fulfilled with substitute shear strains defined in [16], but not with the bilinear displacement interpolation inserted in the transverse shear strains $(1)_3$. Thus the finite element approximation of the shell strains reads

$$\boldsymbol{\varepsilon}_g^h = \begin{bmatrix} \varepsilon_{11}^h \\ \varepsilon_{22}^h \\ 2\varepsilon_{12}^h \\ \kappa_{11}^h \\ \kappa_{22}^h \\ 2\kappa_{12}^h \\ \gamma_1^h \\ \gamma_2^h \end{bmatrix} = \begin{bmatrix} \frac{1}{2}\left(\mathbf{x}_{,1}^h \cdot \mathbf{x}_{,1}^h - \mathbf{X}_{,1}^h \cdot \mathbf{X}_{,1}^h\right) \\ \frac{1}{2}\left(\mathbf{x}_{,2}^h \cdot \mathbf{x}_{,2}^h - \mathbf{X}_{,2}^h \cdot \mathbf{X}_{,2}^h\right) \\ \mathbf{x}_{,1}^h \cdot \mathbf{x}_{,2}^h - \mathbf{X}_{,1}^h \cdot \mathbf{X}_{,2}^h \\ \mathbf{x}_{,1}^h \cdot \mathbf{d}_{,1}^h - \mathbf{X}_{,1}^h \cdot \mathbf{D}_{,1}^h \\ \mathbf{x}_{,2}^h \cdot \mathbf{d}_{,2}^h - \mathbf{X}_{,2}^h \cdot \mathbf{D}_{,2}^h \\ \mathbf{x}_{,1}^h \cdot \mathbf{d}_{,2}^h + \mathbf{x}_{,2}^h \cdot \mathbf{d}_{,1}^h - \mathbf{X}_{,1}^h \cdot \mathbf{D}_{,2}^h - \mathbf{X}_{,2}^h \cdot \mathbf{D}_{,1}^h \\ \mathbf{J}^{-1} \begin{Bmatrix} \frac{1}{2}[(1-\eta)\,\gamma_\xi^B + (1+\eta)\,\gamma_\xi^D \\ \frac{1}{2}[(1-\xi)\,\gamma_\eta^A + (1+\xi)\,\gamma_\eta^C] \end{Bmatrix} \end{bmatrix}. \tag{19}$$

The strains at the midside nodes A, B, C, D of the element are specified as follows

$$\begin{aligned} \gamma_\xi^M &= [\mathbf{x}_{,\xi} \cdot \mathbf{d} - \mathbf{X}_{,\xi} \cdot \mathbf{D}]^M \qquad & M &= B, D \\ \gamma_\eta^L &= [\mathbf{x}_{,\eta} \cdot \mathbf{d} - \mathbf{X}_{,\eta} \cdot \mathbf{D}]^L \qquad & L &= A, C\,, \end{aligned} \tag{20}$$

where the following quantities are given with the bilinear interpolation (12) and (17)

$$\begin{aligned} \mathbf{d}^A &= \tfrac{1}{2}(\mathbf{d}_4 + \mathbf{d}_1) & \mathbf{D}^A &= \tfrac{1}{2}(\mathbf{D}_4 + \mathbf{D}_1) \\ \mathbf{d}^B &= \tfrac{1}{2}(\mathbf{d}_1 + \mathbf{d}_2) & \mathbf{D}^B &= \tfrac{1}{2}(\mathbf{D}_1 + \mathbf{D}_2) \\ \mathbf{d}^C &= \tfrac{1}{2}(\mathbf{d}_2 + \mathbf{d}_3) & \mathbf{D}^C &= \tfrac{1}{2}(\mathbf{D}_2 + \mathbf{D}_3) \\ \mathbf{d}^D &= \tfrac{1}{2}(\mathbf{d}_3 + \mathbf{d}_4) & \mathbf{D}^D &= \tfrac{1}{2}(\mathbf{D}_3 + \mathbf{D}_4) \\ \mathbf{x}_{,\eta}^A &= \tfrac{1}{2}(\mathbf{x}_4 - \mathbf{x}_1) & \mathbf{X}_{,\eta}^A &= \tfrac{1}{2}(\mathbf{X}_4 - \mathbf{X}_1) \\ \mathbf{x}_{,\xi}^B &= \tfrac{1}{2}(\mathbf{x}_2 - \mathbf{x}_1) & \mathbf{X}_{,\xi}^B &= \tfrac{1}{2}(\mathbf{X}_2 - \mathbf{X}_1) \\ \mathbf{x}_{,\eta}^C &= \tfrac{1}{2}(\mathbf{x}_3 - \mathbf{x}_2) & \mathbf{X}_{,\eta}^C &= \tfrac{1}{2}(\mathbf{X}_3 - \mathbf{X}_2) \\ \mathbf{x}_{,\xi}^D &= \tfrac{1}{2}(\mathbf{x}_3 - \mathbf{x}_4) & \mathbf{X}_{,\xi}^D &= \tfrac{1}{2}(\mathbf{X}_3 - \mathbf{X}_4)\,. \end{aligned} \tag{21}$$

3.2 Interpolation of the stress resultants

The independent field of stress resultants $\boldsymbol{\sigma}$ is approximated as follows

$$\begin{aligned} \boldsymbol{\sigma}^h &= \mathbf{N}_\sigma\,\hat{\boldsymbol{\sigma}} & \mathbf{N}_\sigma &= \begin{bmatrix} \mathbf{1}_3 & \mathbf{0} & \mathbf{0} & \mathbf{N}_\sigma^m & \mathbf{0} & \mathbf{0} \\ \mathbf{0} & \mathbf{1}_3 & \mathbf{0} & \mathbf{0} & \mathbf{N}_\sigma^b & \mathbf{0} \\ \mathbf{0} & \mathbf{0} & \mathbf{1}_2 & \mathbf{0} & \mathbf{0} & \mathbf{N}_\sigma^s \end{bmatrix} \\ \mathbf{N}_\sigma^m &= \mathbf{N}_\sigma^b = \mathbf{T}_\sigma^0 \begin{bmatrix} \eta-\bar{\eta} & 0 \\ 0 & \xi-\bar{\xi} \\ 0 & 0 \end{bmatrix} & \mathbf{N}_\sigma^s &= \tilde{\mathbf{T}}_\sigma^0 \begin{bmatrix} \eta-\bar{\eta} & 0 \\ 0 & \xi-\bar{\xi} \end{bmatrix} \end{aligned} \tag{22}$$

where the matrices

$$\mathbf{T}_\sigma^0 = \begin{bmatrix} J_{11}^0 J_{11}^0 & J_{21}^0 J_{21}^0 & 2J_{11}^0 J_{21}^0 \\ J_{12}^0 J_{12}^0 & J_{22}^0 J_{22}^0 & 2J_{12}^0 J_{22}^0 \\ J_{11}^0 J_{12}^0 & J_{21}^0 J_{22}^0 & J_{11}^0 J_{22}^0 + J_{12}^0 J_{21}^0 \end{bmatrix} \qquad \tilde{\mathbf{T}}_\sigma^0 = \begin{bmatrix} J_{11}^0 & J_{21}^0 \\ J_{12}^0 & J_{22}^0 \end{bmatrix} \tag{23}$$

describe the transformation of contravariant tensor components to the local cartesian coordinate system at the element center. The constants $J_{\alpha\beta}^0 = J_{\alpha\beta}(\xi=0,\eta=0)$ are the components of the Jacobian matrix $\mathbf{J}$ in Eq. (14) evaluated at the element center.
The vector $\hat{\boldsymbol{\sigma}} \in R^{14}$ contains 8 parameters for the constant part and 6 parameters for the varying part of the stress field, respectively. The interpolation of the membrane forces and bending moments corresponds to the procedure in [17], see also the original approach for plane stress problems with $\bar{\xi}=\bar{\eta}=0$ in [18]. Due to the constants

$$\bar{\xi} = \frac{1}{A_e}\int\limits_{(\Omega_e)} \xi\, dA \qquad \bar{\eta} = \frac{1}{A_e}\int\limits_{(\Omega_e)} \eta\, dA \qquad A_e = \int\limits_{(\Omega_e)} dA \tag{24}$$

the linear functions are orthogonal to the constant function which yields partly decoupled matrices. The area element $dA = j\, d\xi d\eta$ is given with $j(\xi,\eta) = |\mathbf{X}^h_{,\xi} \times \mathbf{X}^h_{,\eta}|$. Concerning stability of the discrete problem and remarks on the patch test we refer to [14].

3.3 Interpolation of the shell strains

The interpolation of the independent shell strains consists of two parts. The first part with 14 parameters corresponds to the stress interpolation of the last section. The shape functions of the second part with a variable number of parameters β are constructed orthogonal to the stress interpolation. Concerning this point there is a relation to the enhanced strain formulations introduced in [12]. The orthogonality leads to a decoupling of the FE–equations on element level, see the next subsection. Furthermore we refer to [19], where mixed–enhanced interpolation techniques have been investigated. Thus we have

$$\boldsymbol{\varepsilon}^h = \mathbf{N}_\varepsilon\,\hat{\boldsymbol{\varepsilon}}\,, \qquad \mathbf{N}_\varepsilon = [\mathbf{N}_\varepsilon^1, \mathbf{N}_\varepsilon^2]\,, \qquad \hat{\boldsymbol{\varepsilon}} = \begin{bmatrix} \hat{\boldsymbol{\varepsilon}}_1 \\ \hat{\boldsymbol{\varepsilon}}_2 \end{bmatrix}, \qquad \hat{\boldsymbol{\varepsilon}}_1 \in R^{14}\,,\ \hat{\boldsymbol{\varepsilon}}_2 \in R^\beta \tag{25}$$

with the first part

$$\mathbf{N}_\varepsilon^1 = \begin{bmatrix} \mathbf{1}_3 & \mathbf{0} & \mathbf{0} & \mathbf{N}_\varepsilon^{m1} & \mathbf{0} & \mathbf{0} \\ \mathbf{0} & \mathbf{1}_3 & \mathbf{0} & \mathbf{0} & \mathbf{N}_\varepsilon^{b1} & \mathbf{0} \\ \mathbf{0} & \mathbf{0} & \mathbf{1}_2 & \mathbf{0} & \mathbf{0} & \mathbf{N}_\varepsilon^{s1} \\ \mathbf{0} & \mathbf{0} & \mathbf{0} & \mathbf{0} & \mathbf{0} & \mathbf{0} \end{bmatrix}$$

$$\mathbf{N}_\varepsilon^{m1} = \mathbf{N}_\varepsilon^{b1} = \mathbf{T}_\varepsilon^0 \begin{bmatrix} \eta - \bar{\eta} & 0 \\ 0 & \xi - \bar{\xi} \\ 0 & 0 \end{bmatrix}, \qquad \mathbf{T}_\varepsilon^0 = \begin{bmatrix} J_{11}^0 J_{11}^0 & J_{21}^0 J_{21}^0 & J_{11}^0 J_{21}^0 \\ J_{12}^0 J_{12}^0 & J_{22}^0 J_{22}^0 & J_{12}^0 J_{22}^0 \\ 2J_{11}^0 J_{12}^0 & 2J_{21}^0 J_{22}^0 & J_{11}^0 J_{22}^0 + J_{12}^0 J_{21}^0 \end{bmatrix}$$

$$\mathbf{N}_\varepsilon^{s1} = \mathbf{N}_\sigma^s \,. \tag{26}$$

and the second part

$$\mathbf{N}_\varepsilon^2 = \begin{bmatrix} \mathbf{N}_\varepsilon^{m2} & \mathbf{0} & \mathbf{0} \\ \mathbf{0} & \mathbf{N}_\varepsilon^{b2} & \mathbf{0} \\ \mathbf{0} & \mathbf{0} & \mathbf{0} \\ \mathbf{0} & \mathbf{0} & \mathbf{N}_\varepsilon^{z2} \end{bmatrix} \qquad \mathbf{N}_\varepsilon^{m2} = \mathbf{N}_\varepsilon^{b2} = \frac{j_0}{j} \left(\mathbf{T}_\sigma^0\right)^{-T} \mathbf{M}_\alpha \,, \quad \alpha = 2, 4$$

$$\mathbf{M}_2 = \begin{bmatrix} \xi & 0 \\ 0 & \eta \\ 0 & 0 \end{bmatrix} \qquad \mathbf{M}_4 = \begin{bmatrix} \xi & 0 & \xi\eta & 0 \\ 0 & \eta & 0 & \xi\eta \\ 0 & 0 & 0 & 0 \end{bmatrix} \tag{27}$$

with $j_0 = j\,(\xi = 0, \eta = 0)$ and

$$\mathbf{N}_\varepsilon^{z2} = \begin{bmatrix} 1 \end{bmatrix} \quad \text{or} \quad \mathbf{N}_\varepsilon^{z2} = \begin{bmatrix} 1 & 0 \\ 0 & 1 \end{bmatrix} \quad \text{or} \quad \mathbf{N}_\varepsilon^{z2} = \begin{bmatrix} 1 & \xi & \eta & \xi\eta & 0 & 0 & 0 & 0 \\ 0 & 0 & 0 & 0 & 1 & \xi & \eta & \xi\eta \end{bmatrix} \tag{28}$$

The membrane and bending strains may be interpolated in Eq. (27) with linear or bi-linear functions considering 2 or 4 parameters. According to Eq. (28) the thickness strains are interpolated with 1, 2 or 8 parameters. For the first case ε_z and the matrix $\mathbf{A}_2$ in Eq. (4) reduces to

$$\varepsilon_z = \varepsilon_{33}^0 \,, \quad \mathbf{A}_2 = \begin{bmatrix} 0 & 0 & 1 & 0 & 0 & 0 \end{bmatrix}^T \quad . \tag{29}$$

Remark:
Huettel and Matzenmiller developed in [13] a shell theory based on the enhanced assumed strain formulation and employed similar interpolation functions for the thickness strains. The difference is an additional factor J_0/J, which is not necessary in the present case. The factor J denotes the determinant of the Jacobean matrix computed at a point in shell space and J_0 denotes this quantity at the element center.

3.4 Linearized variational formulation

The linearization of the variational equation (10) reads with conservative external loads $\bar{\mathbf{p}}$ and $\bar{\mathbf{t}}$

$$
\begin{aligned}
&L\,[g(\boldsymbol{\theta},\delta\boldsymbol{\theta}),\Delta\boldsymbol{\theta}] := g(\boldsymbol{\theta},\delta\boldsymbol{\theta}) + Dg\cdot\Delta\boldsymbol{\theta} \\
&Dg\cdot\Delta\boldsymbol{\theta} = \int_{(\Omega)} [\delta\boldsymbol{\varepsilon}^T(\mathbf{D}\,\Delta\boldsymbol{\varepsilon} - \Delta\tilde{\boldsymbol{\sigma}}) + \delta\boldsymbol{\sigma}^T(\Delta\boldsymbol{\varepsilon}_g - \Delta\boldsymbol{\varepsilon}_p) + \delta\boldsymbol{\varepsilon}_g^T\Delta\boldsymbol{\sigma} + \Delta\delta\boldsymbol{\varepsilon}_g^T\boldsymbol{\sigma}]\,dA
\end{aligned}
\tag{30}
$$

where

$$
\mathbf{D} := \partial^2_{\boldsymbol{\varepsilon}} W = \int_{h_-}^{h_+} \mathbf{A}^T 4\frac{\partial^2\hat{W}(\mathbf{C})}{\partial\mathbf{C}\,\partial\mathbf{C}}\,\mathbf{A}\,\bar{\mu}\,d\xi^3\,. \tag{31}
$$

The thickness integration in (6) and (31) is performed numerically by summation over layers and with two Gauss integration points for each layer.
Inserting above interpolations for the displacements, stresses and strains yields the finite element approximation

$$
L\,[g(\boldsymbol{\theta}^h,\delta\boldsymbol{\theta}^h),\Delta\boldsymbol{\theta}^h] = \sum_{e=1}^{numel} \begin{bmatrix} \delta\mathbf{v} \\ \delta\hat{\boldsymbol{\varepsilon}} \\ \delta\hat{\boldsymbol{\sigma}} \end{bmatrix}_e^T \left\{ \begin{bmatrix} \mathbf{k}_g & \mathbf{0} & \mathbf{G}^T \\ \mathbf{0} & \mathbf{H} & -\mathbf{F} \\ \mathbf{G} & -\mathbf{F}^T & \mathbf{0} \end{bmatrix} \begin{bmatrix} \Delta\mathbf{v} \\ \Delta\hat{\boldsymbol{\varepsilon}} \\ \Delta\hat{\boldsymbol{\sigma}} \end{bmatrix} + \begin{bmatrix} \mathbf{f}^i - \mathbf{f}^a \\ \mathbf{f}^e \\ \mathbf{f}^s \end{bmatrix} \right\}_e \tag{32}
$$

where *numel* denotes the total number of finite shell elements to discretize the problem. The following element matrices are defined

$$
\begin{aligned}
\mathbf{k}_g &= \int_{(\Omega_e)} \mathbf{k}_\sigma\,dA & \mathbf{f}^i &= \int_{(\Omega_e)} \mathbf{B}^T\boldsymbol{\sigma}^h\,dA = \mathbf{G}^T\,\hat{\boldsymbol{\sigma}} \\
\mathbf{H} &= \int_{(\Omega_e)} \mathbf{N}_\varepsilon^T\,\mathbf{D}\,\mathbf{N}_\varepsilon\,dA & \mathbf{f}^e &= \int_{(\Omega_e)} \mathbf{N}_\varepsilon^T\,\partial_{\boldsymbol{\varepsilon}} W\,dA - \mathbf{F}\,\hat{\boldsymbol{\sigma}} \\
\mathbf{F} &= \int_{(\Omega_e)} \mathbf{N}_\varepsilon^T\,\tilde{\mathbf{N}}_\sigma\,dA & \mathbf{f}^s &= \int_{(\Omega_e)} \mathbf{N}_\sigma^T\,\boldsymbol{\varepsilon}_g^h\,dA - \mathbf{F}^T\,\hat{\boldsymbol{\varepsilon}} \\
\mathbf{G} &= \int_{(\Omega_e)} \mathbf{N}_\sigma^T\,\mathbf{B}\,dA
\end{aligned}
\tag{33}
$$

with $\tilde{\mathbf{N}}_\sigma = [\mathbf{N}_\sigma, \mathbf{0}_{2\times 14}]^T$. The matrices $\mathbf{B}$ and $\mathbf{k}_\sigma$ are specified in Appendix A. The vector of the external loads $\mathbf{f}^a$ corresponds to the one of the standard displacement formulation. The integrals in (24) and (33) are computed numerically using a 2×2 Gauss integration scheme. Due to the orthogonality of the interpolation functions $\tilde{\mathbf{N}}_\sigma$ and $\mathbf{N}_\varepsilon^2$ one obtains

$$
\mathbf{F} = \int_{(\Omega_e)} \begin{bmatrix} \mathbf{N}_\varepsilon^1 \\ \mathbf{N}_\varepsilon^2 \end{bmatrix}^T \tilde{\mathbf{N}}_\sigma\,dA = \begin{bmatrix} \mathbf{F}_1 \\ \mathbf{0} \end{bmatrix} \qquad \mathbf{F}_1 = \begin{bmatrix} A_e\,\mathbf{1}_8 & \mathbf{0} \\ \mathbf{0} & \mathbf{f} \end{bmatrix} \qquad \mathbf{f}_{(6\times 6)} = \begin{bmatrix} \mathbf{f}^m & \mathbf{0} & \mathbf{0} \\ \mathbf{0} & \mathbf{f}^b & \mathbf{0} \\ \mathbf{0} & \mathbf{0} & \mathbf{f}^s \end{bmatrix}. \tag{34}
$$

Using an approximation for j the submatrices in $\mathbf{f}$ can be integrated analytically, see [14]. For the geometrical and physical linear case an analytical integration of all matrices is possible along with a flat projection, see [21] on basis of a Hellinger–Reissner functional.

We continue with $L[g(\boldsymbol{\theta}^h, \delta\boldsymbol{\theta}^h), \Delta\boldsymbol{\theta}^h] = 0$ with $\delta\boldsymbol{\theta}^h \neq \mathbf{0}$ and obtain for each element the following set of equations

$$\begin{aligned} &\mathbf{k}_g\,\Delta\mathbf{v} + \mathbf{G}^T\,\Delta\hat{\boldsymbol{\sigma}} + \mathbf{f}^i - \mathbf{f}^a = \mathbf{r} \\ &\mathbf{H}\,\Delta\hat{\boldsymbol{\varepsilon}} - \mathbf{F}\,\Delta\hat{\boldsymbol{\sigma}} + \mathbf{f}^e = \mathbf{0} \\ &\mathbf{G}\,\Delta\mathbf{v} - \mathbf{F}^T\,\Delta\hat{\boldsymbol{\varepsilon}} + \mathbf{f}^s = \mathbf{0}\,, \end{aligned} \tag{35}$$

where $\mathbf{r}$ denotes the vector of element nodal forces. Since the stresses and strains are interpolated discontinuously across the element boundaries the parameters $\Delta\hat{\boldsymbol{\varepsilon}} = [\Delta\hat{\boldsymbol{\varepsilon}}_1, \Delta\hat{\boldsymbol{\varepsilon}}_2]^T$ and $\Delta\hat{\boldsymbol{\sigma}}$ can be eliminated from the last two equations. For this purpose $(35)_2$ is rewritten

$$\begin{bmatrix} \mathbf{H}_{11} & \mathbf{H}_{12} \\ \mathbf{H}_{21} & \mathbf{H}_{22} \end{bmatrix} \begin{bmatrix} \Delta\hat{\boldsymbol{\varepsilon}}_1 \\ \Delta\hat{\boldsymbol{\varepsilon}}_2 \end{bmatrix} - \begin{bmatrix} \mathbf{F}_1\Delta\hat{\boldsymbol{\sigma}} \\ \mathbf{0} \end{bmatrix} + \begin{bmatrix} \mathbf{f}_1^e \\ \mathbf{f}_2^e \end{bmatrix} = \begin{bmatrix} \mathbf{0} \\ \mathbf{0} \end{bmatrix} \tag{36}$$

introducing the submatrices $\mathbf{H}_{\alpha\beta} = \int_{(\Omega_e)} \mathbf{N}_\varepsilon^{\alpha T}\,\mathbf{D}\,\mathbf{N}_\varepsilon^\beta\,dA$ and $\mathbf{f}_\alpha^e = \int_{(\Omega_e)} \mathbf{N}_\varepsilon^{\alpha T}\,(\partial_{\boldsymbol{\varepsilon}} W - \tilde{\boldsymbol{\sigma}}^h)\,dA$. Static condensation of $\Delta\hat{\boldsymbol{\varepsilon}}_2$ yields

$$\begin{aligned} &\bar{\mathbf{H}}_{11}\,\Delta\hat{\boldsymbol{\varepsilon}}_1 - \mathbf{F}_1\Delta\hat{\boldsymbol{\sigma}} + \bar{\mathbf{f}}_1^e = \mathbf{0} && \bar{\mathbf{H}}_{11} = \mathbf{H}_{11} - \mathbf{H}_{12}\,\mathbf{H}_{22}^{-1}\,\mathbf{H}_{21} \\ &\Delta\hat{\boldsymbol{\varepsilon}}_2 = \mathbf{H}_{22}^{-1}\,(-\mathbf{f}_2^e - \mathbf{H}_{21}\,\Delta\hat{\boldsymbol{\varepsilon}}_1) && \bar{\mathbf{f}}_1^e = \mathbf{f}_1^e - \mathbf{H}_{12}\mathbf{H}_{22}^{-1}\,\mathbf{f}_2^e \end{aligned} \tag{37}$$

as result of a Gauss elimination procedure, see [22]. The set of equations (35) is rewritten using (34) and (37)

$$\begin{aligned} \mathbf{k}_g\,\Delta\mathbf{v} + \mathbf{G}^T\,\Delta\hat{\boldsymbol{\sigma}} + \mathbf{f}^i - \mathbf{f}^a &= \mathbf{r} \\ \bar{\mathbf{H}}_{11}\,\Delta\hat{\boldsymbol{\varepsilon}}_1 - \mathbf{F}_1\,\Delta\hat{\boldsymbol{\sigma}} + \bar{\mathbf{f}}_1^e &= \mathbf{0} \\ \mathbf{G}\,\Delta\mathbf{v} - \mathbf{F}_1^T\,\Delta\hat{\boldsymbol{\varepsilon}}_1 + \mathbf{f}^s &= \mathbf{0}\,, \end{aligned} \tag{38}$$

and solved for the incremental stress and strain parameters

$$\begin{aligned} \Delta\hat{\boldsymbol{\varepsilon}}_1 &= \mathbf{F}_1^{-T}\,(\mathbf{G}\,\Delta\mathbf{v} + \mathbf{f}^s) \\ \Delta\hat{\boldsymbol{\sigma}} &= \mathbf{F}_1^{-1}\,(\bar{\mathbf{H}}_{11}\,\Delta\hat{\boldsymbol{\varepsilon}}_1 + \bar{\mathbf{f}}_1^e)\,. \end{aligned} \tag{39}$$

Inserting (39) in $(38)_1$ yields the tangential element stiffness matrix $\mathbf{k}_T^e$ and the element residual vector $\hat{\mathbf{f}}$. Eq. (32) now reads

$$\begin{aligned} L\,[g(\boldsymbol{\theta}^h, \delta\boldsymbol{\theta}^h), \Delta\boldsymbol{\theta}^h] &= \sum_{e=1}^{numel} \delta\mathbf{v}^T(\mathbf{k}_T^e\,\Delta\mathbf{v} + \hat{\mathbf{f}}) = 0 \\ \mathbf{k}_T^e &= \mathbf{G}^T\,\hat{\mathbf{H}}\,\mathbf{G} + \mathbf{k}_g \qquad\qquad \hat{\mathbf{H}} = \mathbf{F}_1^{-1}\,\bar{\mathbf{H}}_{11}\,\mathbf{F}_1^{-T} \\ \hat{\mathbf{f}} &= \mathbf{G}^T\,(\hat{\boldsymbol{\sigma}} + \hat{\mathbf{H}}\,\mathbf{f}^s + \mathbf{F}_1^{-1}\,\bar{\mathbf{f}}_1^e) - \mathbf{f}^a \end{aligned} \tag{40}$$

Summarizing, besides the elimination of a variable number of parameters $\Delta\hat{\boldsymbol{\varepsilon}}_2$ in (36) by static condensation [22], the only matrix which has to be inverted is $\mathbf{F}_1$, which means little effort due to its diagonal structure.

The global matrices are obtained by standard assembly procedures. The solution of the system of equations yields the increment $\Delta \mathbf{v}_k = [\Delta \mathbf{u}_k, \Delta \boldsymbol{\beta}_k]^T$. Here, one has to consider the transformation

$$\Delta \boldsymbol{\omega}_K = \mathbf{T}_{3K}\, \Delta \boldsymbol{\beta}_K \qquad \mathbf{T}_{3K} = \begin{cases} \mathbf{1}_3 & \text{for nodes on shell intersections} \\ [\mathbf{a}_{1K}, \mathbf{a}_{2K}]_{(3\times 2)} & \text{for all other nodes} \end{cases}$$

$$\Delta \boldsymbol{\beta}_k = \begin{cases} [\Delta\beta_{xk}, \Delta\beta_{yk}, \Delta\beta_{zk}]^T & \text{for nodes on shell intersections} \\ [\Delta\beta_{1k}, \Delta\beta_{2k}]^T & \text{for all other nodes} \end{cases} \tag{41}$$

which is discussed in [20]. Thus the element possesses six degrees of freedom at nodes on intersections and five at all other nodes. In this context we also refer to Reference [23].
The update of the nodal displacements is performed in a standard way on the structural level,

$$\begin{aligned} \mathbf{u}_K &\Longleftarrow \mathbf{u}_K + \Delta \mathbf{u}_K \\ \boldsymbol{\omega}_K &\Longleftarrow \boldsymbol{\omega}_K + \Delta \boldsymbol{\omega}_K \end{aligned} \qquad \hat{\boldsymbol{\sigma}} \Longleftarrow \hat{\boldsymbol{\sigma}} + \Delta \hat{\boldsymbol{\sigma}} \qquad \hat{\boldsymbol{\varepsilon}} \Longleftarrow \hat{\boldsymbol{\varepsilon}} + \Delta \hat{\boldsymbol{\varepsilon}}\,, \tag{42}$$

whereas the stress and strain parameters are updated on the element level using (39). For this purpose the matrices which are necessary for the update have to be stored for each element.

4 Examples

The derived element formulation has been implemented in an extended version of the general purpose finite element program FEAP, see Taylor [24]. Some numerical examples are chosen to demonstrate the accurate behavior of the proposed element.
One purpose of the numerical examples is, to show that the element approximates the three-dimensional constitutive behavior correctly. The results of the present formulation are compared to a solid shell element formulation presented in [25]. The solid shell element incorporates a three dimensional material law. There is no plane stress condition imposed within the element formulation, the stress state is determined by the equilibrium condition. Furthermore comparative calculations are performed employing a shell element, where the zero stress condition in thickness direction is satisfied iteratively at each integration point, see [4]. However, for typical shell problems all formulations should lead to similar results for the overall behavior, which is investigated in the range of finite elastic and finite plastic strain problems. Different results between these element formulations are discussed in detail.
The first example investigates the patch test. Fulfillment is fundamental to ensure convergence within a finite element calculation. Next, a channel section cantilever beam is considered to account for shell intersections. The third example is concerned with a stretching problem where finite elastic strains arise. It includes the analysis of a stability problem. The fourth and fifth example are concerned with large plastic strains. A square plate is subjected to a transverse dead load, which leads to sharp folding in the corners. Due to the high bending stresses large strains are obtained in these regions. The fifth example analyzes a metal forming process where large plastic stretching strains occur.

4.1 Membrane and bending patch test

First we investigate the element behavior within a constant membrane and bending patch test as it is depicted in Fig. 2, see also [26]. A rectangular plate of length a and width b is supported at three corners. We consider in-plane loading and bending loading denoted by load case 1 and 2, respectively. Both, membrane and bending patch test are fulfilled by the present element with constant normal forces $n_x = 1, n_y = n_{xy} = 0$ (load case 1) and constant bending moments $m_x = m_y = m_{xy} = 1$ (load case 2).

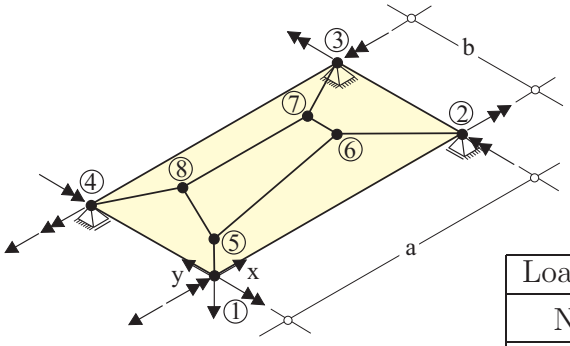

$a = 40 \qquad E = 10^6$
$b = 20 \qquad \nu = 0.3$
$h = 0.1$

Load case	1	2		
Node	$\bar{F}_x$	$\bar{F}_z$	$\bar{m}_x$	$\bar{m}_y$
1	-20	-2	20	-10
2	0	0	20	10
3	0	0	-20	10
4	-20	0	-20	-10

Figure 2: Rectangular plate, patch of 5 elements

4.2 Channel section cantilever with plasticity

This example demonstrates that the present formulation is able to handle shell intersections. The channel section is a well known test example, see for instance [27, 28, 29]. The system is

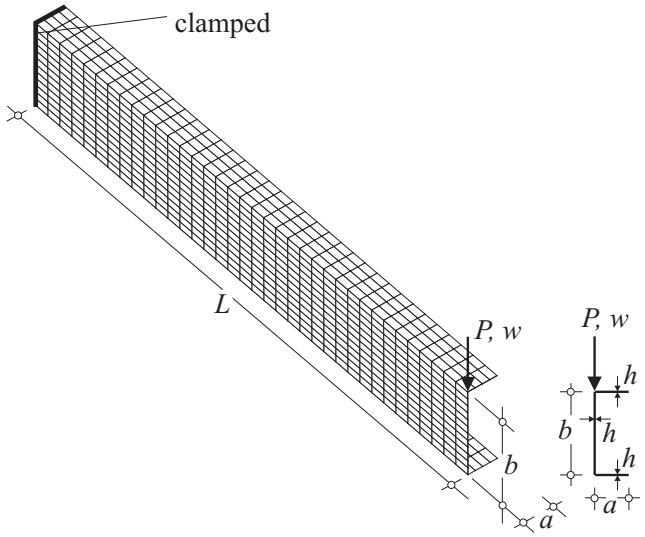

Figure 3: Channel section cantilever system and finite element model

depicted in Fig. 3 and the dimensions between center lines are given as $L = 36\,\text{in}$, $a = 2\,\text{in}$, $b = 6\,\text{in}$, $h = 0.05\,\text{in}$ and $E = 10^7\,\text{lb/in}^2$, $\nu = 0.333$. Here, a material is used, which allows moderate elasto-plastic strains. According to [27] the ideal plastic deformation is characterized by the yield stress $y_0 = 5 \cdot 10^3\,\text{lb/in}^2$ without any hardening.

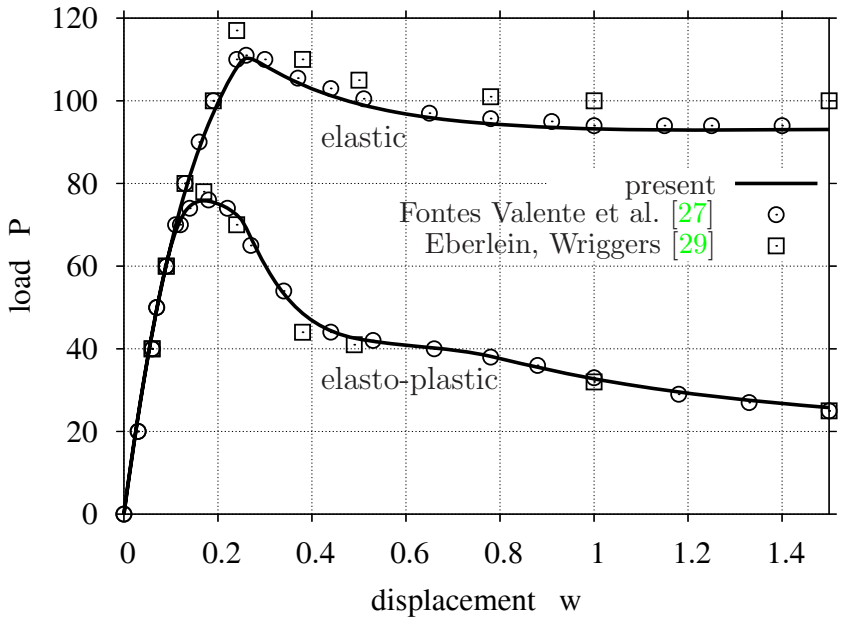

Figure 4: Channel section cantilever: load deflection curve for the vertical displacement w

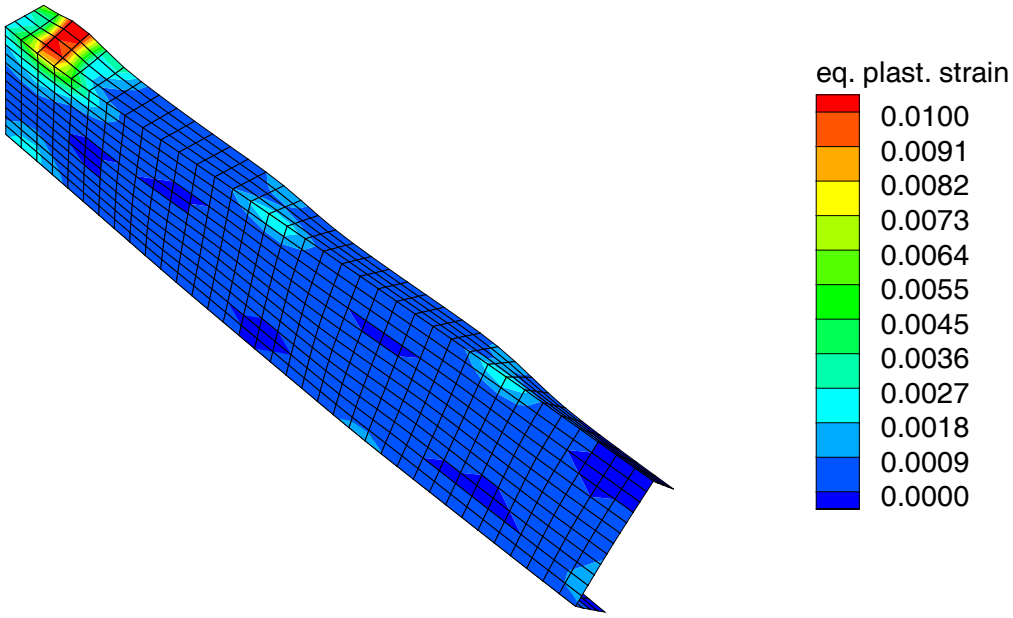

Figure 5: Deformed configuration of the channel section cantilever with a plot of the equivalent plastic strains at the outside surface

One end of the beam is clamped, on the free end a tip load P is subjected. The calculation is performed using an arclength method with displacement control, where the displacement w in direction of the load is controlled. The finite element model is depicted in Fig. 3 and consists out of 36 elements in longitudinal direction of the beam and 4/12/4 elements in circumferential direction of the cross section. Further mesh refinement shows no significant influence on the displacement response. For the thickness integration two Gauss quadrature points are employed in total.
In Fig. 4 the load P is plotted versus the deflection w for a pure elastic and for the elasto-plastic material behavior. In the elastic case the curves coincide very well with the solution of [27]. Also for the elasto-plastic behavior good agreement between the different solutions is observed. In Fig. 5 the deformed configuration with a plot of the equivalent plastic strains is shown. A comparison with [27] shows good agreement.

4.3 Stretching of a rubber sheet

This example has been analyzed previously e.g. in [30, 10]. Here, we use this example to demonstrate that the present element formulation approximates the thickness strains within finite elastic strains correctly. Therefore the results are compared to those of the solid shell element.

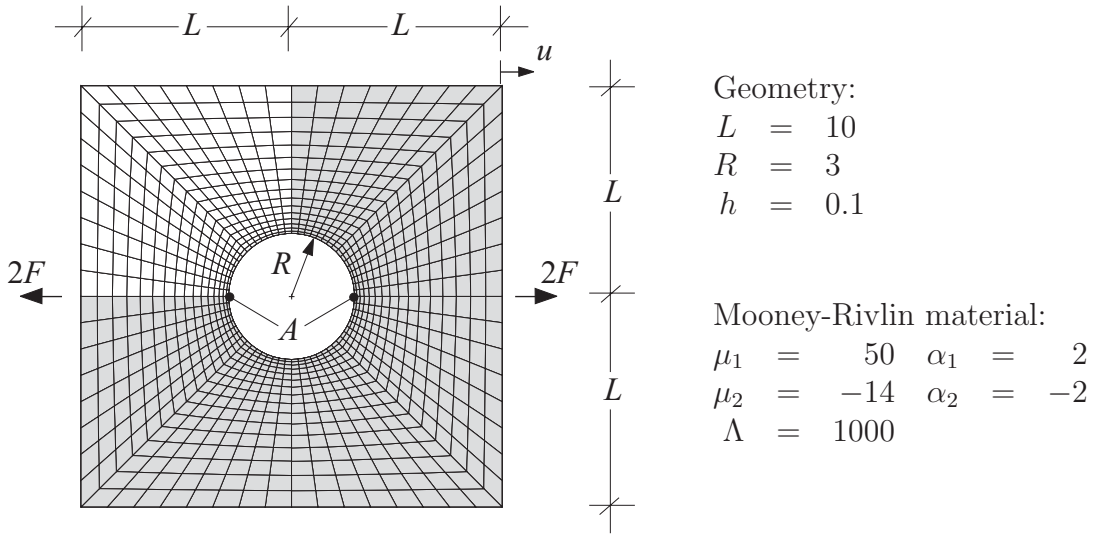

Figure 6: Geometry and material data of the rubber sheet with hole

A square sheet with a hole is subjected to a stretching load. The incompressible material response is governed by a Mooney-Rivlin model (see Appendix B.1). Fig. 6 shows system and material parameters. With respect to symmetry only one quarter of the system is discretized with finite elements. At the left and right edge the degrees of freedom are linked together, such that same horizontal but no vertical displacements occur. The sheet is stretched up to twice of the original length, see Fig. 7. At the inner edge of the hole a stability problem is observed due to the occurrence of compression stresses. In order to follow the secondary equilibrium path, a perturbation load $10^{-7}\,F$ is added at point A perpendicular to the sheet plane, see Fig. 6. The secondary path is characterized by an out-of-plane deflection w.

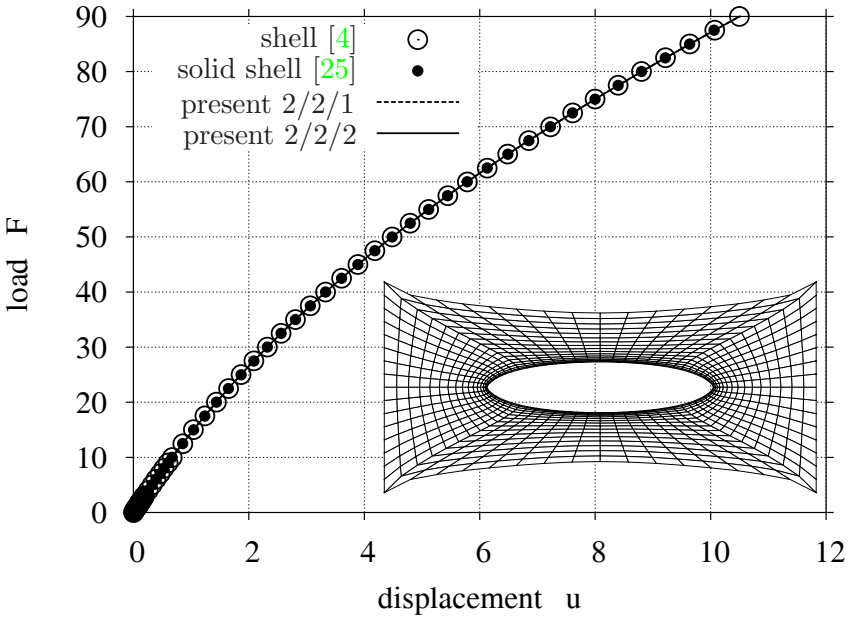

Figure 7: Load deflection curve for the horizontal displacement u and deformed rubber sheet with hole at $F = 90$

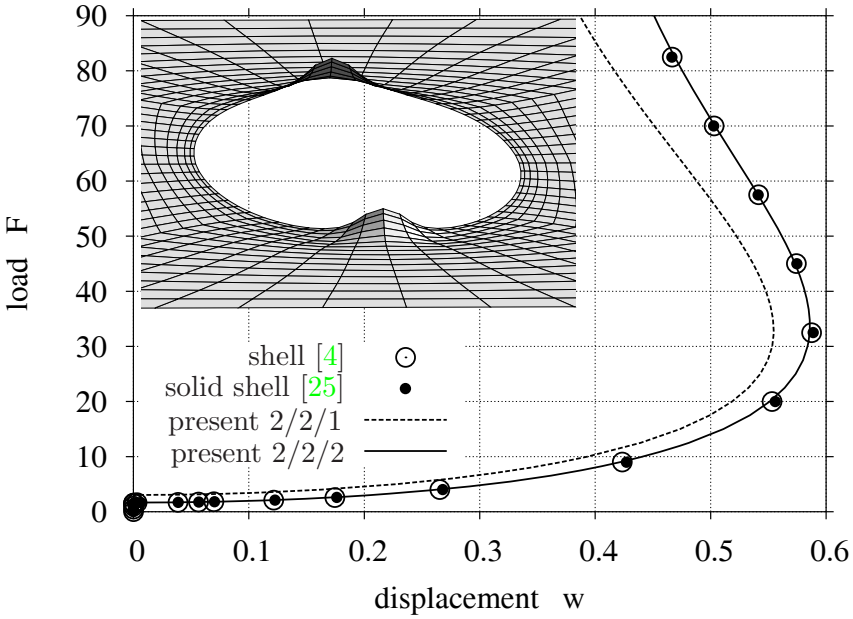

Figure 8: Load deflection curve for the out of plane displacement w and perspective view of the hole of the deformed rubber sheet at $F = 90$

In Fig. 7 the load F is depicted versus the horizontal displacement u. The present element is used with two sets of interpolation parameters for membrane/bending/thickness, see Eqs. (27, 28). Results are presented for the sets 2/2/1 and 2/2/2 and compared to calculations employing the solid shell element [25] with only one element through the thickness and the shell element [4]. For both element types a two point Gauss quadrature through the thickness is

used. In Fig. 8 the load F is plotted versus the out of plane deflection w at point A . The present formulation 2/2/1 considers only a constant approximation of the thickness strain. It can be seen that this simplification leads to an overestimation of the buckling load. The parameter set 2/2/2 denotes a linear approximation of the thickness strain, see Eq. (28). It leads to results which coincide very well with the shell and the solid shell element in diagrams Figs. 7, 8. The example demonstrates that the present element is able to approximate problems with finite elastic strains correctly.

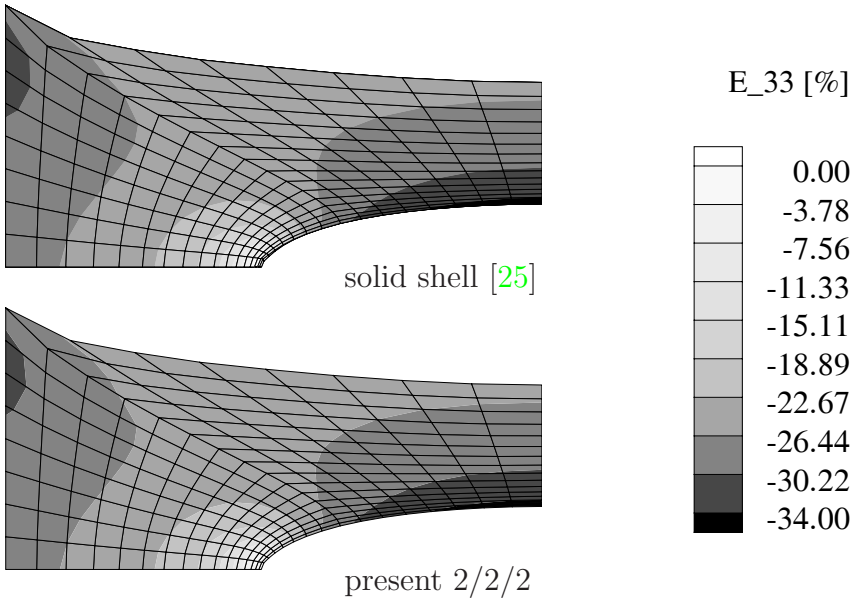

Figure 9: Thickness strain of the deformed rubber sheet with hole at $F = 90$; only one quarter of the deformed configuration is shown

load increment	iteration	1	2	3	4	5	6	7	8
$F = 2 \rightarrow 5$	shell [4]	10^{0}	10^{-1}	10^{-2}	10^{-1}	10^{-3}	10^{-4}	10^{-6}	10^{-9}
	solid shell [25]	10^{0}	10^{1}	10^{0}	10^{-1}	10^{-3}	10^{-8}		
	present	10^{0}	10^{-1}	10^{-1}	10^{-3}	10^{-5}	10^{-10}		
load increment	iteration	1	2	3	4	5	6	7	8
$F = 10 \rightarrow 50$	shell [4]	no convergence							
	solid shell [25]	10^{1}	10^{2}	10^{1}	10^{1}	10^{-1}	10^{-3}	10^{-8}	
	present	10^{1}	10^{1}	10^{0}	10^{-1}	10^{-2}	10^{-4}	10^{-8}	

Table 1: Convergence of the residual during equilibrium iteration

Fig. 9 shows a plot of the strain in thickness direction. The strain is evaluated at the upper layer of the Gauss integration points for the present element and for the solid shell element. The strain distributions agree very well, which confirms that the present element leads to the same results as the solid shell element.
In Tab. 1 the convergence rates of the global equilibrium iteration for different load steps are listed. The zero stress condition for the shell element [4] is imposed with a local Newton

iteration. It is observed that the present formulation is very robust with respect to the load step size.

4.4 Square plate

This example demonstrates that the present element formulation is able to analyze extreme bending situations where large plastic strains occur. It is a popular example for shell formulations within finite elasto-plastic strains, see e. g. [29]. The plate is supported in z-direction along the edges and loaded by a transversal dead load q in z-direction. A finite strain plasticity model based on the work of [31] is applied and summarized in Appendix B.2. Here, perfect plasticity without hardening is assumed. The geometry and material data are shown in Fig. 10. With respect to symmetry only one quarter of the system is modeled by 32 $\times$ 32 elements. A further mesh refinement does not lead to a significant change of the results. For the thickness integration 5 layers of equal thickness are employed with a two point Gauss quadrature for each layer. It is remarked that 2 layers would be enough for the calculation of the load deflection curve. Here, 5 layers are employed for the plot of the thickness strain to be very close to the upper surface.

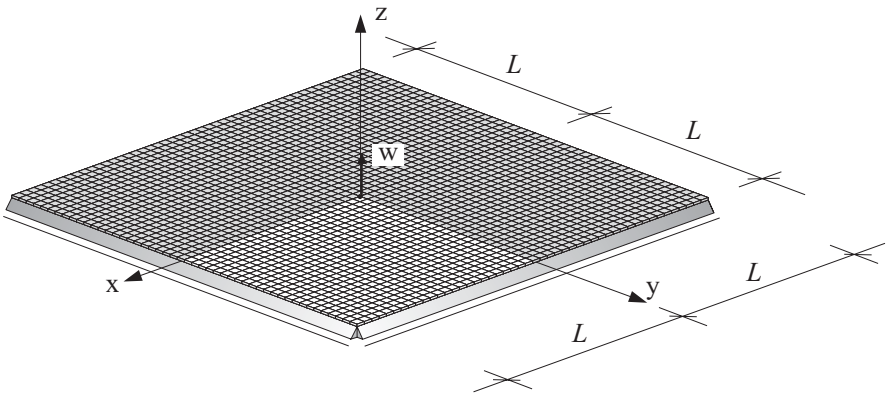

Geometry:
$L = 254$
$h = 2.54$

Load:
$q = \lambda \cdot 10^{-2}$

Material:
$E = 69000$
$\nu = 0.3$
$y_0 = 248$

Figure 10: Geometry and material data of the square plate

The associated load deflection diagram of the midpoint deflection is depicted in Fig. 11. As can be seen the results of the present formulation are in very good agreement with results using the solid shell element.
The influence of the strain interpolations (27, 28) is investigated next. The impact of the bending and membrane interpolations is discussed in [20], where 2 and 4 parameters for both terms are used. As a result it is concluded that 2 parameters for both, the bending and the membrane strains, are sufficient to obtain reasonable results. Here, the impact of the thickness interpolation is analyzed by comparing the deflections of the loaded plate. Therefore a regular and an irregular finite element mesh are taken into account and are illustrated in Fig. 12. Again parameter sets are defined for membrane, bending and thickness interpolations.

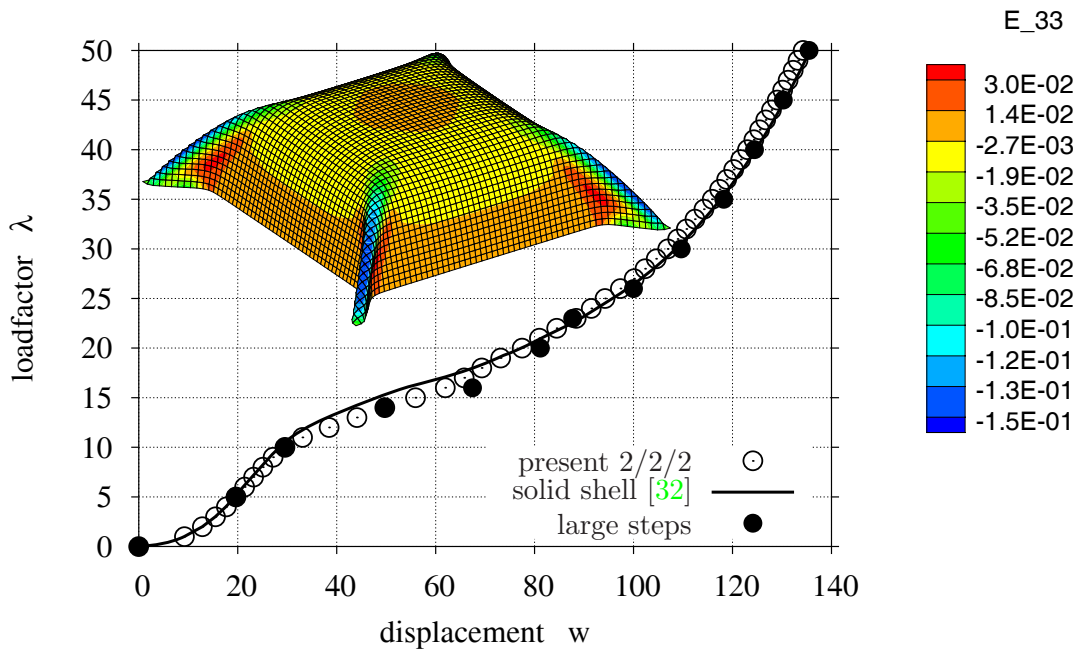

Figure 11: Load deflection curve of the vertical displacement w at the midpoint of the plate, deformed mesh with a plot of the thickness strain at the upper surface

The vertical midpoint displacements of the plate for different thickness interpolations are listed in Tab. 2. The constant approximation of the thickness strains with the parameter set 2/2/1 converges to a much smaller deflection as the linear approximation 2/2/2. The reason for this behavior is that the thickness strain is not correctly approximated in bending dominated situations. The bi-linear interpolation with 8 parameters leads not to significantly different results than the 2/2/2 parameter set, which holds for the regular as well as for the irregular finite element mesh. Thus, the use of 2 parameters for the interpolation of thickness strains could be recommended.

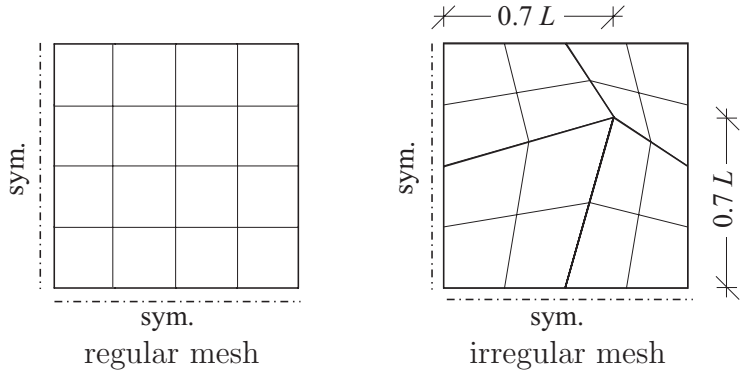

Figure 12: Applied finite element meshes of a quarter of the plate for parameter study

regular FE-mesh	2/2/1	2/2/2	2/2/8
4×4	0.775	0.785	0.787
8×8	0.838	0.881	0.883
16×16	0.852	0.939	0.944
32×32	0.856	0.976	0.980
64×64	0.857	0.992	0.994
128×128	0.857	0.999	1.004

irregular FE-mesh	2/2/1	2/2/2	2/2/8
4×4	0.776	0.788	0.790
8×8	0.835	0.873	0.874
16×16	0.851	0.929	0.933
32×32	0.856	0.970	0.975
64×64	0.857	0.990	0.992
128×128	0.857	1.000	1.000

Table 2: Midpoint deflection w normalized with w= 30.28 for different parameters and finite element meshes at $q = 10^{-1}$

4.5 Conical shell

This example is selected to demonstrate the ability of the developed shell element formulation to deal with strongly non-linear situations. The geometrical data are taken from Başar and

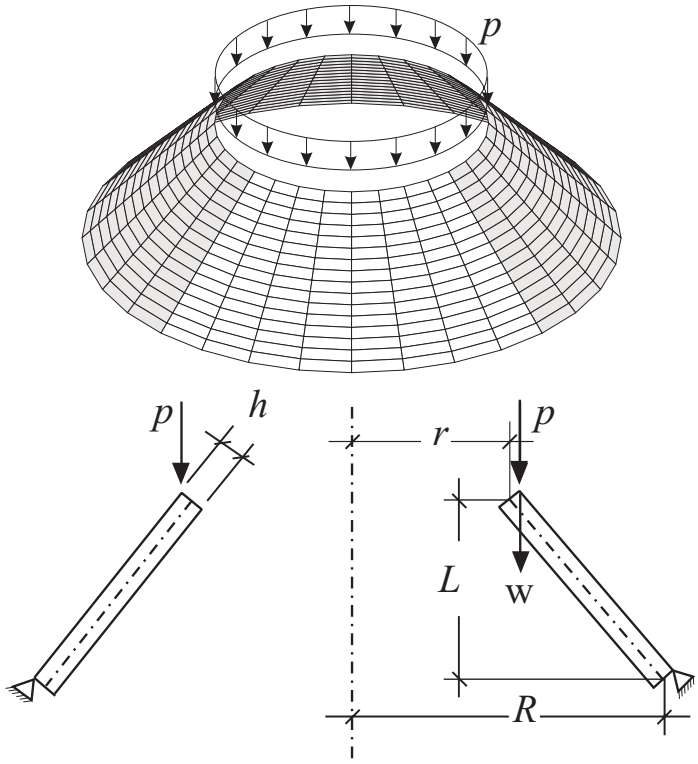

Geometry:

r	=	1
R	=	2
L	=	1
h	=	0.1

Material:

E	=	206.9
ν	=	0.29
y_0	=	0.45
y_∞	=	0.715
ς	=	0.12924
ϱ	=	16.93

Load: p

Figure 13: Finite element mesh with geometrical and material data

Itskov [33], who investigated this problem using an Ogden material. Here, the elasto-plastic material model according to Appendix B.2 is used. All necessary material and geometrical data are depicted in Fig. 13. Regarding to [33] the problem is slightly modified due to eccentric loading and support conditions, see Fig. 13. The boundary conditions are modeled exactly by the solid shell [25] as well as by the present finite shell element when considering the integration limits $h_- = -h$ and $h_+ = 0$ in Eqs. (6),(31). For the present shell integration through the thickness is performed using 4 layers with two Gauss quadrature points for each layer. Due to symmetry, only one quarter of the shell is modeled with 8 elements in circumferential direction and 16 elements in axial direction. For the solid shell one element through the thickness is employed. Only rotationally symmetric deformations are considered within the calculation. Two parameters for the membrane, bending as well as thickness strain interpolation are used, see Eqs. (27), (28).

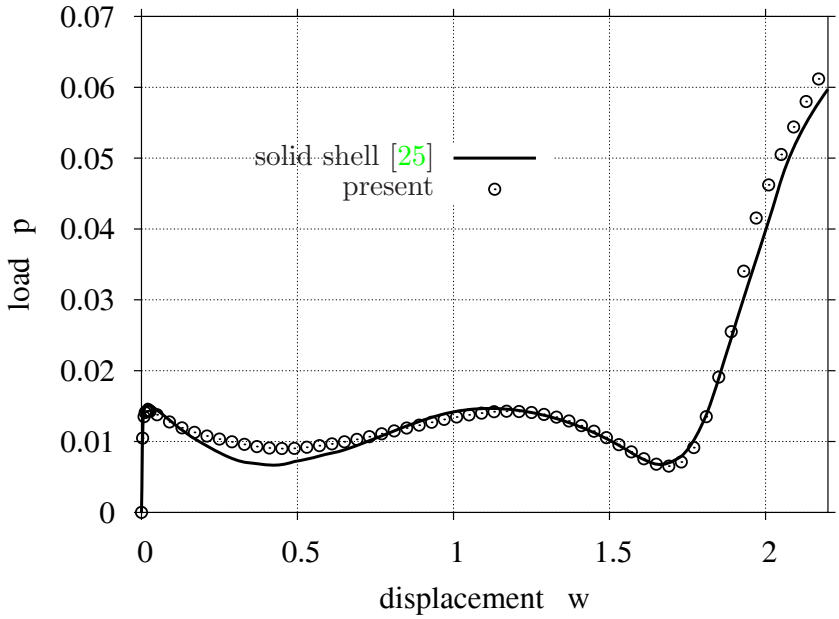

Figure 14: Load deflection diagram: load p versus vertical displacement w of the upper outer edge

The non-linear behavior is computed using an arclength algorithm with displacement control for the vertical displacement w at the upper edge. The results are depicted in a load deflection diagram, see Fig. 14. It can be seen that the displacement response of the present formulation and the solid shell formulation [25] agree very well. Small differences occur with respect to the fact that the solid shell approach is only integrated with 2 Gauss quadrature points through the total thickness.
The load is increased until $w = 0.02$, where the elastic limit load is reached. Hence a rolling process starts at the top of the conical shell. A further stability point is traced at $w \approx 1.2$. Here, a global snap through behavior is observed. A local minimum of the load deflection curve is attained at $w \approx 1.7$. Then a stable path with increasing loads due to stiffening effects arises. Deformed meshes at characteristic points are shown in Fig. 15.

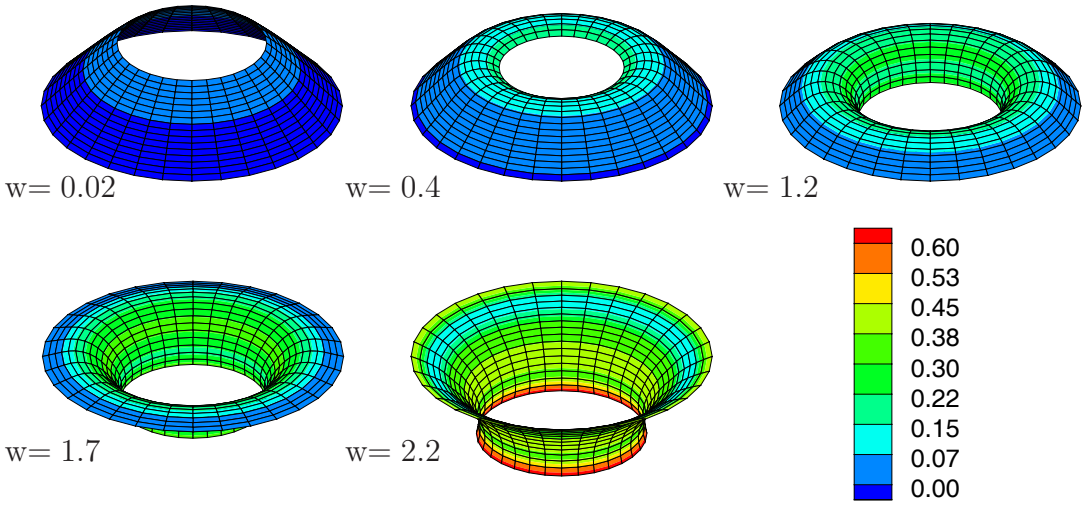

Figure 15: Deformed meshes with a plot of the equivalent plastic strains evaluated at the initial outside surface

5 Conclusions

The present paper deals with the structural analysis of thin shells using a mixed hybrid shell element. Using a three field variational principle appropriate interpolation functions for the independent mechanical fields are described. The approximation of the shell strains is improved introducing additional interpolation functions. The investigations show that two parameters for the membrane part and two parameters for the bending part are sufficient. As special feature independent thickness strains are included which allows consideration of arbitrary nonlinear three-dimensional constitutive equations. Interpolation functions for the thickness strains are presented with one, two and eight parameters. The tests show that, a) one parameter may lead only in special situations to correct results, b) two parameters are sufficient to have reasonable converged results, whereas c) eight parameters lead only to negligible improvements in comparison to two parameters. As a conclusion one can recommend the use of two parameters for the thickness interpolation. The presented examples show furthermore that especially for finite deformations the new formulation allows very large load steps and requires essentially less equilibrium iterations in comparison to displacement based elements.

Appendix

A Finite element matrices B and $\mathbf{k}_\sigma$

The matrices $\mathbf{B}$ and $\mathbf{k}_\sigma$ have been derived in [14]. In this appendix the results are summarized. The finite element approximation of the shell strains (19) yields with (17 - 21)

$$\begin{bmatrix} \delta\varepsilon^h_{11} \\ \delta\varepsilon^h_{22} \\ 2\delta\varepsilon^h_{12} \\ \delta\kappa^h_{11} \\ \delta\kappa^h_{22} \\ 2\delta\kappa^h_{12} \\ \delta\gamma^h_1 \\ \delta\gamma^h_2 \end{bmatrix} = \sum_{I=1}^{4} \begin{bmatrix} N_{I,1}\,\mathbf{x}^T_{,1} & \mathbf{0} \\ N_{I,2}\,\mathbf{x}^T_{,2} & \mathbf{0} \\ N_{I,1}\,\mathbf{x}^T_{,2} + N_{I,2}\,\mathbf{x}^T_{,1} & \mathbf{0} \\ N_{I,1}\,\mathbf{d}^T_{,1} & N_{I,1}\,\mathbf{b}^T_{I1} \\ N_{I,2}\,\mathbf{d}^T_{,2} & N_{I,2}\,\mathbf{b}^T_{I2} \\ N_{I,1}\,\mathbf{d}^T_{,2} + N_{I,2}\,\mathbf{d}^T_{,1} & N_{I,1}\,\mathbf{b}^T_{I2} + N_{I,2}\,\mathbf{b}^T_{I1} \\ \mathbf{J}^{-1} \begin{Bmatrix} N_{I,\xi}\,\mathbf{d}^T_M \\ N_{I,\eta}\,\mathbf{d}^T_L \end{Bmatrix} & \mathbf{J}^{-1} \begin{Bmatrix} N_{I,\xi}\,\xi_I\,\mathbf{b}^T_M \\ N_{I,\eta}\,\eta_I\,\mathbf{b}^T_L \end{Bmatrix} \end{bmatrix} \begin{bmatrix} \delta\mathbf{u}_I \\ \delta\boldsymbol{\beta}_I \end{bmatrix} \tag{43}$$

$$\delta\boldsymbol{\varepsilon}^h_g = \sum_{I=1}^{4} \mathbf{B}_I\,\delta\mathbf{v}_I$$

with $\mathbf{b}_{I\alpha} = \mathbf{T}_I^T\,\mathbf{x}_{,\alpha}$, $\mathbf{b}_M = \mathbf{T}_I^T\,\mathbf{x}^M_{,\xi}$, $\mathbf{b}_L = \mathbf{T}_I^T\,\mathbf{x}^L_{,\eta}$ and $\mathbf{T}_I = \mathbf{W}_I^T\mathbf{H}_I\mathbf{T}_{3I}$, where

$$\begin{aligned} \mathbf{W}_I &= \operatorname{skew}\mathbf{d}_I \\ \mathbf{H}_I &= \mathbf{1} + \frac{1-\cos\omega_I}{\omega_I^2}\,\boldsymbol{\Omega}_I + \frac{\omega_I - \sin\omega_I}{\omega_I^3}\,\boldsymbol{\Omega}_I^2 \\ \mathbf{T}_{3I} &= \begin{cases} \mathbf{1} & \text{for nodes on shell intersections} \\ [\mathbf{a}_{1I}, \mathbf{a}_{2I}]_{(3\times 2)} & \text{for all other nodes}\,. \end{cases} \end{aligned} \tag{44}$$

Thus one obtains $\mathbf{B} = [\mathbf{B}_1, \mathbf{B}_2, \mathbf{B}_3, \mathbf{B}_4]$.

The second variation of the shell strains yields with the vector of the independent stress resultants $\boldsymbol{\sigma}^h$ the product

$$\begin{aligned} \Delta\delta\boldsymbol{\varepsilon}_g^{hT}\boldsymbol{\sigma}^h &= \sum_I^4 \sum_K^4 \delta\mathbf{v}_I^T\,\mathbf{k}_{\sigma IK}\,\Delta\mathbf{v}_K \\ &= \sum_I^4 \sum_K^4 \begin{bmatrix} \delta\mathbf{u}_I \\ \delta\boldsymbol{\beta}_I \end{bmatrix}^T \begin{bmatrix} \hat{n}_{IK}\mathbf{1} & (\hat{m}_{IK} + \hat{q}^{uw}_{IK})\mathbf{T}_K \\ (\hat{m}_{IK} + \hat{q}^{wu}_{IK})\mathbf{T}_I^T & \delta_{IK}\,\hat{\mathbf{M}}_I \end{bmatrix} \begin{bmatrix} \Delta\mathbf{u}_K \\ \Delta\boldsymbol{\beta}_K \end{bmatrix} \end{aligned} \tag{45}$$

where

$$
\begin{aligned}
\hat{n}_{IK} &= n^{11}\,N_{I,1}\,N_{K,1} + n^{22}\,N_{I,2}\,N_{K,2} + n^{12}\,(N_{I,1}\,N_{K,2} + N_{I,2}\,N_{K,1}) \\
\hat{m}_{IK} &= m^{11}\,N_{I,1}\,N_{K,1} + m^{22}\,N_{I,2}\,N_{K,2} + m^{12}\,(N_{I,1}\,N_{K,2} + N_{I,2}\,N_{K,1}) \\
\hat{q}^{uw}_{IK} &= \tfrac{1}{2}(q^{\xi}\,N_{I,\xi}\,f^{1}_{IK} + q^{\eta}\,N_{I,\eta}\,f^{2}_{IK}) \\
\hat{q}^{wu}_{IK} &= \tfrac{1}{2}(q^{\xi}\,N_{K,\xi}\,f^{1}_{IK} + q^{\eta}\,N_{K,\eta}\,f^{2}_{IK}) \\
\hat{\mathbf{M}}_I &= \mathbf{T}^{T}_{3I}\,\mathbf{H}^{T}_{I}\,\mathbf{M}_I\,\mathbf{H}_I\,\mathbf{T}_{3I} \\
\mathbf{M}_I &= \frac{1}{2}(\mathbf{d}_I \otimes \mathbf{h}_I + \mathbf{h}_I \otimes \mathbf{d}_I) + \frac{1}{2}(\mathbf{t}_I \otimes \boldsymbol{\omega}_I + \boldsymbol{\omega}_I \otimes \mathbf{t}_I) + c_{10}\mathbf{1} \\
\mathbf{t}_I &= -c_3\,\mathbf{b}_I + c_{11}\,(\mathbf{b}_I \cdot \boldsymbol{\omega}_I)\,\boldsymbol{\omega}_I \\
\mathbf{b}_I &= \mathbf{d}_I \times \mathbf{h}_I \\
\mathbf{h}_I &= m^{11}\,N_{I,1}\,\mathbf{x}^{h}_{,1} + m^{22}\,N_{I,2}\,\mathbf{x}^{h}_{,2} + m^{12}\,(N_{I,2}\,\mathbf{x}^{h}_{,1} + N_{I,1}\,\mathbf{x}^{h}_{,2}) \\
&\quad + q^{\xi}\,N_{I,\xi}\,\xi_I \mathbf{x}^{M}_{,\xi} + q^{\eta}\,N_{I,\eta}\,\eta_I \mathbf{x}^{L}_{,\eta} \qquad (46) \\
c_{10} &= \bar{c}_{10}\,(\mathbf{b}_I \cdot \boldsymbol{\omega}_I) - (\mathbf{d}_I \cdot \mathbf{h}_I) \\
\bar{c}_{10} &= \frac{\sin\omega_I - \omega_I}{2\omega_I\,(\cos\omega_I - 1)} \\
c_3 &= \frac{\omega_I\,\sin\omega_I + 2\,(\cos\omega_I - 1)}{\omega_I^2\,(\cos\omega_I - 1)} \\
c_{11} &= \frac{4\,(\cos\omega_I - 1) + \omega_I^2 + \omega_I \sin\omega_I}{2\,\omega_I^4\,(\cos\omega_I - 1)}
\end{aligned}
$$

$$
[f^{1}_{IK}] = \begin{bmatrix} 1 & 1 & 0 & 0 \\ 1 & 1 & 0 & 0 \\ 0 & 0 & 1 & 1 \\ 0 & 0 & 1 & 1 \end{bmatrix} \qquad [f^{2}_{IK}] = \begin{bmatrix} 1 & 0 & 0 & 1 \\ 0 & 1 & 1 & 0 \\ 0 & 1 & 1 & 0 \\ 1 & 0 & 0 & 1 \end{bmatrix} \qquad \begin{bmatrix} q^{\xi} \\ q^{\eta} \end{bmatrix} = \mathbf{J}^{-T} \begin{bmatrix} q^{1} \\ q^{2} \end{bmatrix}.
$$

The allocation of the midside nodes to the corner nodes is given by

$$
(I, M, L) \in \{(1, B, A); (2, B, C); (3, D, C); (4, D, A)\}\,. \qquad (47)
$$

The geometrical matrix $\mathbf{k}_{\sigma}$ is determined with the submatrices $\mathbf{k}_{\sigma IK}$.

B Non-linear constitutive equations

B.1 Hyper-elastic material

Following [34, 35] the strain energy function is given by

$$
W_{0S} = \sum_{r=1}^{2} [\frac{\mu_r}{\alpha_r}(\lambda_1^{\alpha_r} + \lambda_2^{\alpha_r} + \lambda_3^{\alpha_r} - 3) - \mu_r\,\ln(J)] + \frac{\Lambda}{4}(J^2 - 1 - 2\,\ln(J)) \qquad (48)
$$

with

$$J = \lambda_1 \lambda_2 \lambda_3 \quad . \tag{49}$$

Here λ_i are the principal stretches of the elastic material, which are evaluated by solving the eigenvalue problem

$$(\mathbf{C} - \lambda_A^2 \mathbf{1}) \mathbf{N}^A = \mathbf{0} \quad \text{with} \quad A = 1, 2, 3 \quad . \tag{50}$$

Furthermore $\mathbf{N}^A$ denotes the eigenvector and the right Cauchy-Green tensor $\mathbf{C}$ is obtained from $\mathbf{C} = 2\mathbf{E} + \mathbf{1}$. The material parameter Λ is the Lamé constant, which may be computed from the shear modulus $\mu = (\mu_1 \alpha_1 + \mu_2 \alpha_2)/2$ and the bulk modulus κ as $\Lambda = \kappa - 2/3\mu$. For a large value of Λ it can be interpreted as a penalty factor and the incompressibility condition is approximately fulfilled, $\det \mathbf{F} = \lambda_1 \lambda_2 \lambda_3 \approx 1$.

B.2 Finite strain J_2-plasticity model

The applied plasticity model for finite strains is restricted to isotropic material behavior. The numerical realization of the finite strain J_2-plasticity model is proposed in several papers; see e.g. [31], [36] and the references therein. The finite deformation plasticity model is based on a multiplicative decomposition of the deformation gradient $\mathbf{F} = \mathbf{F}^e \, \mathbf{F}^p$ in an elastic and plastic part. Due to the Lagrangean formulation of the variational equations the plasticity model is formulated using the right Cauchy-Green tensor. With $\mathbf{C}^p = \mathbf{F}^{p\,T} \mathbf{F}^p$ the eigenvalue problem

$$(\mathbf{C} - \lambda_A^{e\,2} \mathbf{C}^p) \, \hat{\mathbf{N}}^A = \mathbf{0} \quad \text{with} \quad \hat{\mathbf{N}}^A \cdot \mathbf{C}^p \, \hat{\mathbf{N}}^B = \delta^{AB} \tag{51}$$

yields the elastic stretches λ_A^e. The elastic strain energy function is defined as

$$W_{el} = \frac{\Lambda}{2} [\varepsilon_1^e + \varepsilon_2^e + \varepsilon_3^e]^2 + \mu [(\varepsilon_1^e)^2 + (\varepsilon_2^e)^2 + (\varepsilon_3^e)^2] \quad \text{with} \quad \varepsilon_A = ln[\lambda_A^e] \quad . \tag{52}$$

Here Λ and μ are the Lamé constant and the shear modulus, respectively. These are given in terms of the Young's modulus E and Poisson's ratio ν as $\Lambda = \frac{E\,\nu}{(1+\nu)(1-2\nu)}$ and $\mu = \frac{E}{2(1+\nu)}$. The evolution law of the plastic strains and the internal variable are derived from the principle of maximum plastic dissipation. A Lagrangean formulation of the plastic flow rule is given as

$$\dot{\mathbf{C}}^p = 2 \, \lambda \, \mathbf{C}^p \, (\mathbf{F}^{-1} \frac{\partial \phi}{\partial \boldsymbol{\tau}} \mathbf{F}), \qquad \dot{\alpha} = \lambda \frac{\partial \phi}{\partial q} \tag{53}$$

where λ denotes the Lagrange multiplier, $\boldsymbol{\tau}$ is the Kirchhoff stress and α, q are conjugate internal hardening variables. The yield criterion ϕ is of a von Mises type with exponential isotropic hardening

$$\phi = \sqrt{\frac{3}{2} \boldsymbol{\tau}^D \cdot \boldsymbol{\tau}^D} - (y_0 + \varsigma \, \alpha + (y_\infty - y_0)(1 - \exp[-\varrho \, \alpha])) \quad . \tag{54}$$

In this equation y_0 denotes the initial yield stress, ς determines the linear hardening and y_∞, ϱ describe exponential hardening. The deviatoric Kirchhoff stress tensor is denoted by $\boldsymbol{\tau}^D$. An implicit exponential integration algorithm of the evolution equations (53) along with the strain energy (52), introduced in [31], leads to an additive model as in the linear theory.

References

[1] TJR Hughes and E Carnoy. Nonlinear finite element shell formulation accounting for large membrane strains. *Computer Methods in Applied Mechanics and Engineering*, 39:69–82, 1983.

[2] R de Borst. The zero–normal–stress condition in plane–stress and shell elastoplasticity. *Communications in Applied Numerical Methods*, 7:29–33, 1991.

[3] E Dvorkin, D Pantuso, and E Repetto. A formulation of the MITC4 shell element for finite strain elasto-plastic analysis. *Computer Methods in Applied Mechanics and Engineering*, 125:17–40, 1995.

[4] S Klinkel and S Govindjee. Using finite strain 3d-material models in beam and shell elements. *Engineering Computations*, 19:902–921, 2002.

[5] Y Basar and Y Ding. Shear deformation models for large-strain shell analysis. *International Journal of Solids and Structures*, 34:1687–1708, 1997.

[6] B Brank, J Korelc, and A Ibrahimbegovic. Nonlinear shell models with seven kinematic parameters. *Computer Methods in Applied Mechanics and Engineering*, 194:2336–2362, 2002.

[7] C Sansour. A theory and finite element formulation of shells at finite deformations involving thickness change: circumventing the use of a rotation tensor. *Archive of Applied Mechancis*, 65:194–216, 1995.

[8] B Brank. Nonlinear shell models with seven kinematic parameters. *Computer Methods in Applied Mechanics and Engineering*, 194:2336–2362, 2005.

[9] N Büchter, E Ramm, and D Roehl. Three–dimensional extension of non–linear shell formulation based on the enhanced assumed strain concept. *International Journal for Numerical Methods in Engineering*, 37:2551–2568, 1994.

[10] P Betsch, F Gruttmann, and E Stein. A 4–node finite shell element for the implementation of general hyperelastic 3d–elasticity at finite strains. *International Journal for Numerical Methods in Engineering*, 37:2551–2568, 1994.

[11] M Bischoff and E Ramm. On the physical significance of higher order kinematic and static variables in a three–dimensional shell formulation. *International Journal of Solids and Structures*, 37:6933–6960, 2000.

[12] JC Simo and MS Rifai. A class of mixed assumed strain methods and the method of incompatible modes. *International Journal for Numerical Methods in Engineering*, 29:1595–1638, 1990.

[13] C Huettel and A Matzenmiller. Consistent discretization of thickness strains in thin shells including 3d-material models. *Communications in Numerical Methods in Engineering*, 15:283–293, 1999.

[14] W Wagner and F Gruttmann. A robust nonlinear mixed hybrid quadrilateral shell element. *International Journal for Numerical Methods in Engineering*, 64:635–666, 2004.

[15] AE Green and PM Naghdi. On the derivation of shell theories by direct approach. *Journal of Applied Mechanics*, 41:173–176, 1974.

[16] E Dvorkin and KJ Bathe. A continuum mechanics based four node shell element for general nonlinear analysis. *Engineering Computations*, 1:77–88, 1984.

[17] JC Simo, DD Fox, and MS Rifai. On a stress resultant geometrically exact shell model. Part ii: The linear theory; computational aspects. *Computer Methods in Applied Mechanics and Engineering*, 73:53–92, 1989.

[18] TTH Pian and K Sumihara. Rational approach for assumed stress finite elements. *International Journal for Numerical Methods in Engineering*, 20:1685–1695, 1984.

[19] EP Kasper and RL Taylor. A mixed-enhanced strain method Part ii: Geometrically nonlinear problems. *Computerts & Structures*, 75:251–260, 2000.

[20] F Gruttmann and W Wagner. Structural analysis of composite laminates using a mixed hybrid shell element. *Computational Mechanics*, 37:479–497, 2006.

[21] F Gruttmann and W Wagner. A linear quadrilateral shell element with fast stiffness computation. *Computer Methods in Applied Mechanics and Engineering*, 194:4279–4300, 2005.

[22] RD Cook, DS Malkus, and ME Plesha. *Concepts and Applications of Finite Element Analysis*. John Wiley & Sons, New York, 3 edition, 1989.

[23] JC Simo. On a stress resultant geometrically exact shell model. Part vii: Shell intersections with 5/6-dof finite element formulations. *Computer Methods in Applied Mechanics and Engineering*, 108:319–339, 1993.

[24] RL Taylor. Feap - manual. *http:\\www.ce.berkeley\ ∼rlt\feap\manual.pdf*, online.

[25] S Klinkel, F Gruttmann, and W Wagner. A robust non-linear solid shell element based on a mixed variational formulation. *Computer Methods in Applied Mechanics and Engineering*, 195:179–201, 2006.

[26] RH MacNeal and RL Harder. A proposed standard set of problems to test finite element accuracy. *Finite Elements in Analysis and Design*, 1:3–20, 1985.

[27] R.A. Fontes Valente, M.P.L. Parente, R.M. Natal Jorge, J.M.A. Cesar de Sa, and J.J. Gracio. Enhanced transverse shear strain shell formulation applied to elasto-plastic deformation problems. *International Journal for Numerical Methods in Engineering*, 62:1360–1398, 2005.

[28] J. Chroscielewski and W. Witkowski. Four-node semi-EAS element in six-field nonlinear theory of shells. *International Journal for Numerical Methods in Engineering*, 68:1137–1179, 2006.

[29] R Eberlein and P Wriggers. Finite element concepts for finite elastoplastic strains and isotropic stress response in shells: theoretical and computational analysis. *Computer Methods in Applied Mechanics and Engineering*, 171:243–279, 1999.

[30] H Parisch. Efficient non-linear finite element shell formulation involving large strains. *Engineering Computations*, 3:121–126, 1986.

[31] JC Simo. Algorithms for static and dynamic multiplicative plasticity that preserve the classical return mapping schemes of the infinitesimal theory. *Computer Methods in Applied Mechanics and Engineering*, 99:61–112, 1992.

[32] S Klinkel, W Wagner, and F Gruttmann. A continuum based 3d-shell element for computation of laminated structures and finite strain plasticity problems. In Topping BHV, editor, *Computational Techniques for Materials, Composites and Composite Structures*, pages 297–310. Civil-Comp Press, 2000.

[33] Y Basar and M Itskov. Finite element formulation of the Ogden material model with application to rubber-like shells. *International Journal for Numerical Methods in Engineering*, 42:1279–1305, 1998.

[34] L Treloar. Stress-strain data for vulcanised rubber under various types of deformation. *Transactions of the Faraday Society*, 40:59–70, 1944.

[35] R Ogden. Large deformation isotropic elasticity – on the correlation of theory and experiment for compressible rubberlike solids. *Proceedings of Royal Society London*, A328:567–583, 1972.

[36] C Miehe and E Stein. A canonical model of multiplicative elasto-plasticity formulation and aspects of the numerical implementation. *European Journal of Mechanics*, A 11:25–43, 1992.